

**GENETIC ENGINEERING OF BACTERIOPHAGE AND ITS APPLICATIONS
FOR BIOMIMETIC MATERIALS**

by

Soo-Kwan Lee

SUBMITTED TO BIOLOGICAL ENGINEERING DIVISION IN PARTIAL
FULFILLMENT OF THE REQUIREMENTS FOR THE DEGREE OF

**DOCTOR OF PHILOSOPHY IN BIOLOGICAL ENGINEERING
AT THE
MASSACHUSETTS INSTITUTE OF TECHNOLOGY**

September 2006

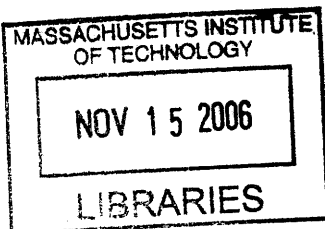
©2006 Soo-Kwan Lee. All right reserved.

The author hereby grants to MIT permission to reproduce
and to distribute publicly paper and electronic
copies of this thesis document in whole or in part
in any medium now known or hereafter created.

Signature of Author: _____
Biological Engineering Division
August 10, 2006

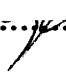
Certified by: _____
Angela M. Belcher
Professor of Biological Engineering
Thesis Supervisor


Accepted by: _____
Ram Sasisekharan
Professor of Biological Engineering
Chairman, Committee for Graduate Students




ARCHIVES

Thesis committee:

Angela M. Belcher..........Professor of Biological Engineering
Massachusetts Institute of Technology

K. Dane Wittrup..........Professor of Biological Engineering
Massachusetts Institute of Technology

Scott Manalis..........Professor of Biological Engineering
Massachusetts Institute of Technology

GENETIC ENGINEERING OF BACTERIOPHAGE AND ITS APPLICATIONS FOR BIOMIMETIC MATERIALS

by
Soo-Kwan Lee

Submitted to Biological Engineering Division
on August 01, 2006 in Partial Fulfillment of the
Requirements for the Degree of Philosophy in
Biological Engineering

Abstract

Filamentous bacteriophage (M13) are excellent biological build block due to their multiple peptide display system including type 8 (complete peptide display at pVIII) and type 83 (complete peptide display at both pVIII and pIII) display systems. Unlike the phagemid systems, the advantage of these systems is that we can get homogenous peptide display on pVIII resulting in uniform placement of selected molecules as well as defined length and width. In this thesis, type 8 and type 83 phage were constructed and used as biological scaffolds to meet the following four specific aims. First, the self-assembly of engineered M13 bacteriophage as a template for Co-Pt crystals was demonstrated. A phage library with an octapeptide library on the major coat protein (pVIII) was used for selection of binders to cobalt ions. Fibrous structures with directionally ordered phage were obtained by interaction with cobalt ions. Co-Pt alloys were synthesized on the fibrous scaffold, and their magnetic properties were characterized. The mineralization showed organized nanoparticles on fibrous bundles with superparamagnetic properties. Second, an *in vitro* molecular selection method in non-biological conditions for inorganic synthesis was introduced. A phage display peptide library which is resistant to ethanol was constructed and used for selection against titania in 90% ethanol. The selected peptide, with a conserved basic amino acid sequence, promotes nanoparticle formation (~ 60 nm) during titania synthesis by the traditional sol-gel method. Third, storage of proteins in smectically aligned phage film was demonstrated. β -galactosidase and a green fluorescent protein variant were stored in the phage film with increased stability. In addition, streptavidin conjugated phycoerythrin were aligned in a S1 phage film, in which streptavidin binding peptides are displayed at the end of the phage particles. The alignment showed increased fluorescent intensity of phycoerythrin molecules. Finally, the potential of type 8 and type 83 phage as a nano-structural scaffold were studied for device application. An Au binding peptide was selected using type 8 phage library. Self-assembly of gold particles on phage was observed. In addition, type 83 phage which display both streptavidin binding peptide at pIII and Au binding peptide at pVIII were constructed for complex assembly of both Au nanoparticles and streptavidin conjugated nanoparticles. Genetically engineered bacteriophage show promise for application including biologically compatible materials and functional bio-inorganic hybrid materials

Thesis Supervisor: Angela M. Belcher
Title: Professor of Biological Engineering

This thesis is dedicated to my family,
My parents, Ho-Jae Lee and Young-Soon Park
My wife, Soo Youn Yim
My son, Sean Y. Lee
My son, Justin Y. Lee

Acknowledgements

I would like to thank my advisor Angela M Belcher for her support, advice and inspiration. She has always given me both thoughtful recommendations and the opportunity to make my own decisions.

Professor K. Dane Wittrup and Scott Manalis, members of my thesis committee, are always supportive. I would like to thank professor K. Dane Wittrup for his valuable insight in various aspects of my research, and professor Scott Manalis for his positive feedback on my experiments.

I wish to thank everyone in the Belcher Lab, especially my collaborators, Seung-Wuk Lee, Dong Soo Yun, Chung, Yu, Kitae, Stephen, and Jifa. Specially thanks to Dr. Yun for helpful discussion and TEM images. Thanks Sreekar for enjoyable discussion and encouragement. I would also like to thank Elisabeth L. Shaw for discussion about XPS analysis.

This thesis would not have been possible if not for the generous support of my wife. She had always cheered and encouraged me to keep studies. I thank my wife, Soo Youn Yim, for the confidence in my works.

Finally, I would like to acknowledge the financial support provided by Army Research Office, Institute of Collaborative Biotechnologies, and the David and Lucile Packard Foundation.

Table of Contents

List of Tables.....	9
List of Figures.....	10
CHAPTER 1: Introduction.....	17
1.1. Thesis Objectives.....	17
1.2. Bacteriophage as Template of Inorganics.....	18
1.3. Directional Alignment of Phage Particles.....	21
1.4. Three Dimensional Self-Assembly of Biological Molecules.....	22
1.5. Sol-Gel Method for TiO ₂ Particle and Phage Stability.....	23
1.6. Background on Inorganic Nano-materials.....	25
CHAPTER 2: Cobalt Ions Mediated Self-Assembly of Genetically Engineered Bacteriophage for Biomimetic Co-Pt Hybrid Materials.....	27
2.1. Abstract.....	27
2.2. Introduction.....	28
2.3. Material and Methods.....	30
2.3.1. Materials.....	30
2.3.2. Type 8 phage library.....	30
2.3.3. Biopanning against cobalt ion.....	32
2.3.4. Synthesis of Co-Pt on phage templates.....	32
2.3.5. Characterization.....	32
2.4. Result and discussion.....	33
2.5. Conclusion.....	43
CHAPTER 3: Phage Displayed Peptide Selection for TiO₂ in a Non-Biological Environment.....	44
3.1. Abstract.....	44

3.2.	Introduction.....	45
3.3.	Material and Methods.....	47
3.3.1.	Selection of ethanol resistant phage using pVIII phage library.....	47
3.3.2.	Infectivity assay in ethanol.....	48
3.3.3.	Ethanol resistant pIII phage library.....	48
3.3.4.	Biopanning against TiO ₂	49
3.3.5.	Synthesis of TiO ₂ with the selected peptide.....	50
3.3.6.	Characterization.....	50
3.4.	Result and discussion.....	51
3.5.	Conclusion.....	58
 CHAPTER 4: Alignment and Storage of Biological Molecules in Phage Film		59
4.1.	Abstract.....	59
4.2.	Introduction.....	60
4.3.	Material and Methods.....	61
4.3.1.	β-galactosidase stability in phage film.....	61
4.3.2.	GFPuv stability in phage film.....	62
4.3.3.	Alignment and stability of phycoerythrin in phage film.....	62
4.4.	Result and discussion.....	63
4.5.	Conclusion.....	68
 CHAPTER 5: Assembly of Inorganic Nanoparticles using Genetically Engineered Bacteriophage		69
5.1.	Abstract.....	69
5.2.	Introduction.....	70
5.3.	Material and Methods.....	72
5.3.1.	Biopanning against Au surface.....	72
5.3.2.	pIII modification of p8#9 phage.....	72

5.3.3.	Assembly of Au nanoparticles on p8#9 phage.....	73
5.3.4.	Fabrication of nano-architectures.....	73
5.4.	Result and discussion.....	74
5.5.	Conclusion.....	77
CHAPTER 6: Summary and Conclusions.....		78
Appendix A: Construction of M13SK vector		81
Appendix B: Construction of type 83 phage		84
References.....		86

List of Tables

Table 1. Percentage of amino acids in type 8 phage library.35

Table B1. PCR of type 3 phage for construction of type 83 phage84

List of Figures

Figure 1. M13 phage display systems. Type 3 or type 8 phage can be obtained by genetically engineering of N-terminal region of gene III (gIII) or gene VIII (gVIII). Type 8+8 phage contains restricted amount of modified pVIII by introducing phagemid with genetically engineered gVIII. For type 83 phage, both gIII and gVIII are modified.19

Figure 2. Biopanning with Type 8 phage library. Inorganic target surface is immersed into solution containing type 8 phage library, washed away the excess phage, and eluted using 0.2M Glycine-HCl (pH 2.2). The eluted phage is amplified, and the process is repeated several times to find the tightest binders. The number of plaques can be titered, and each plaques is amplified and sequenced to determine the selected peptide sequence.20

Figure 3. Liquid crystal phases of phage. (a) nematic, (b) smectic A, and (c) smectic C phase, where the axis of the rod-like molecules are tilted.22

Figure 4. A schematic diagram illustrating formation of Co-Pt hybrid material using a self-assembled phage framework (orange dots = cobalt ions, black dots = Co-Pt).29

Figure 5. Scheme for construction of type 8 phage library in M13SK. Schematic shows the restriction sites for cloning DNA library into M13SK. X = any randomized amino acids.31

Figure 6. (a) Photograph of cobalt mediated fibrils in solution using wild-type (left), anti-Co²⁺ (center), and no phage (right). (b) Optical microscopy image and (c) TEM image of the fibrils (from center sample). Inset: directional placement of phage particle along the bundle (d) Cross-POM image of (b).36

Figure 7. Synthesis of Co-Pt nanoparticles on fibrous phage template. (a) Solution after nucleation and growth of Co-Pt with wild-type (left), anti-Co²⁺ (center), and no phage (right). (b) SEM image of the anti-Co²⁺ sample after freeze-drying. (c) TEM image of the anti-Co²⁺ sample. (d) TEM image showing bundled phage. Inset: SAED pattern of Co-Pt. (e) HRTEM of individual Co-Pt nanoparticles showing lattice fringes and a lattice spacing (inset). (f) Distribution of particle diameters from TEM images (average particle size = 2.3 nm).38

Figure 8. TEM image of Co-Pt without phage (a) and with wild-type phage (b).39

Figure 9. (a) STEM image of Co-Pt nanoparticles prepared on the fibrous phage bundle. Atomic ratios of Co and Pt on fibrous structure are shown. (b) Co and (c) Pt map showing distribution of Co and Pt.40

Figure 10. ZFC (solid rectangle) and FC (open circle) magnetization as a function of temperature. Sample was cooled with (FC) or without (ZFC) magnetic field (100 Oe) to 5K, and then heated up to 300K.41

Figure 11. Magnetization versus applied magnetic field at 5K (solid rectangle) and 300K (open circle).42

Figure 12. Fit for the Langevin function at 300K (red line).43

Figure 13. A schematic diagram for peptide selection in ethanol. Phage which can survive in ethanol are selected by incubation in 90% ethanol and amplification of surviving phage three times. A pIII library is made by genetic engineering of the surviving phage, and used to select against TiO₂ substrate in 90% ethanol. After four rounds of the biopanning process, the selected phage are characterized by sequencing of the phage DNA.47

Figure 14. Scheme for construction of ethanol resistant pIII phage library. dsDNA of ethanol resistant phage with “EGVSNPAM” insert at N-terminal of pVIII are modified to have octamer peptide library with Gly-Gly-Gly linker at N-terminal of pIII. (X = random amino acids).49

Figure 15. Ethanol resistant phage. (a) pVIII displayed peptide sequences with numbers of observed sequences (left panel), (b) infectivity of predominant resistant phage in series of different time and percent of ethanol.52

Figure 16. Selected peptide sequence in 90% ethanol against TiO₂ crystal. Conserved basic amino acids (red); Arginine (R), Lysine (K), and Histidine (H). Peptides were named by sequenced order (left panel).53

Figure 17. TiO₂ particles with peptide. (a)TEM image with diffraction (inset), (b) HRTEM showing (101) and (004) facets, (c) line-scan using STEM for elements of Ti (red), O (green), S (blue), (d) SEM image of precipitated particles.55

Figure 18. TEM image of TiO₂ without K1 peptide showing irregular particles which is linked together.55

Figure 19. XPS of TiO₂ precipitants. (a) Survey of TiO₂ with and without K1. Additional peaks for N and S were observed in sample with K1 peptide (red line).57

Figure 20. High resolution XPS spectra of Ti 2p peak of TiO₂ with K1(a) and without K1 (b).57

Figure 21. High resolution XPS spectra of Oxygen 1s spectra with K1 (a) and without K1 peptide.58

Figure 22. Scheme for alignment of streptavidin conjugated phycoerythrin in smectic phage film. Streptavidin can bind to an end of a phage particle which displays streptavidin binding peptides at N-terminal of pIII.61

Figure 23. Effect of glucose/sucrose and phage on β -galactosidase activity during storage at room temperature. Day 0 represents the recovered activity after drying in desiccator.64

Figure 24. Confocal microscopy images of fluorescent GFPuv in the viral film after one day from their fabrication with same GFPuv and phage concentration and with variation of concentration of glucose / sucrose; (A) 5mg/ml / 50mg/ml, (B) 2.5mg/ml / 25mg/ml, and (C) without glucose and sucrose.65

Figure 25. (a) Photograph of phycoerythrin-phage film, (b) POM image of phycoerythrin-phage film (scale bar: 100 μ m), (c) fluorescence image of phycoerythrin-phage film, and (d) phycoerythrin-phage film on glass slide, showing one micrometer striped patterns (scale bar: 10 μ m).66

Figure 26. Effect of glucose/sucrose and phage on aligned phycoerythrin during storage at room temperature. Day 0 represents the recovered activity after drying in desiccator.67

Figure 27. Scheme for the type 83 phage for assembly of Au nanoparticle on pVIII and streptavidin conjugated CdSe nanoparticles on pIII.71

Figure 28. (a) the suspension of Au nanoparticles with and without phage. Blank control sample contains Au nanoparticles alone, and wild-type and p8#17 phage are used as control. p8#9 phage is the selected Au binding phage. TEM image of blank control sample (b), wild-type (c), p8#17 (d), and p8#9 (e) phage. Wild-type and p8#17 phage were stained by using uranyl-acetate (1%).75

Figure 29. TEM images of various nanoarchitectures templated by #9S1 phage. (a and b) Assembly of Au nanoparticles (5 nm) at pVIII and streptavidin conjugated Au nanoparticles (15 nm) at pIII. (c) CdSe quantum dot (15 nm) at pIII and Au nanoparticles at pVIII. (d and e) example of complex structure in which streptavidin conjugated Au nanoparticle (15 nm) are bridge two or three phage particles.76

Figure A1. Restriction site map of M13SK. M13KE vector was modified. *Pst I* and *BamHI* sites were added, and *Pst I* at Multi cloning site was deleted.82

Figure A2. Overlap extension PCR for pVIII cloning sites. Two individual PCR products with mutation sites were obtained. The two PCR products were extended and amplified with 5'-M13KE-1179 and 3'-M13KE-2 primers.83

Figure B1. Construction of Type 83 phage. PCR product which contains Pst I and BamH I restriction site was obtained. The region between BamH I and Eag I was cloned to type 8 phage dsDNA. The dsDNA of type 83 phage contains DNA sequence for peptide display at both pIII (orange) and pVIII (red).85

CHAPTER 1: Introduction

1.1. Thesis Objectives

Precise recognition and self-assembly of biological components are required in cells for their structure and proper function, such as actin filaments, microtubules, and chromatin. The biological recognition is mediated by the electrostatic, hydrophobic, hydrogen bonding, and Van Der Waals interaction. Due to the high specificity on interaction that translates to the nanoscales, biological molecules are potential building blocks for nucleation and self-assembly of inorganic materials. The ‘bottom-up’ biomimetic fabrication with biological templates, such as DNA,[1] amphiphilic peptides,[2] and artificial proteins,[3] has been introduced for supramolecular architectures. The research objective of this thesis is to apply engineered type 8 (completely modified pVIII with selected peptides) and type 83 (both completely modified pVIII and pIII) bacteriophage display systems as a biological scaffold. Unlike the phagemid systems, the advantage of these systems is that we can get homogenous display on pVIII resulting in the nucleation of inorganic crystals with uniform placement as well as defined length and width. Phage particles can be aligned by controlling the flow in a particular direction due to its rod-like shape. In addition, the alignment can also be controlled by the concentration of phage particles. Cross-binder to pVIII could increase local concentration of phage particles and cause directionally

ordered alignment. The self-assembled phage particles can potentially be applied as advanced biological building block and can be used to align inorganic and biological materials. The pVIII modification is known to affect the stability of phage in aqueous and non-aqueous solutions. By increasing the stability of phage particles in non-aqueous solutions, it could be possible to select peptides in these types of solutions.

Therefore, I constructed genetically engineered type 8 and type 83 phage, and I used these as biological scaffolds to meet the following specific aims: (1) cobalt ion mediated self-assembly of genetically engineered bacteriophage for biomimetic Co-Pt hybrid material. (2) phage displayed peptide selection for TiO₂ in a non-biological environment. (3) Alignment and storage of biological molecules in phage film and (4) Assembly of inorganic nanoparticles using genetically engineered bacteriophage.

1.2. Bacteriophage as Template of Inorganics.

Virus such as tobacco mosaic virus (TMV) [4] and cowpea chlorotic mottle virus (CCMV) [5] were used as biological nanoscale scaffolds to nucleate inorganics. This nucleation was due to regular surface pattern of charged amino acid residues, such as glutamate, aspartate, arginine, and lysine. However, peptides, which are selected for inorganic compounds using phage display peptide library,[6] were used successfully for nucleation and growth control of the inorganic nanoparticles in aqueous solution at room temperature.[7, 8] Filamentous bacteriophage (f1, fd, and M13) is excellent biological building block itself due to its multiple peptide display system (Figure 1) and its controllable length. Wild-type filamentous bacteriophage is approximately 930 nm in length

and ~ 6 nm in diameter. The phage surface is consisted of five capsid proteins (pIII, pVI, pVII, pVIII, and pIV). pIII (approximately 5 molecules) is commonly used to display foreign molecules (natural peptide, random peptides, protein, and protein domains).

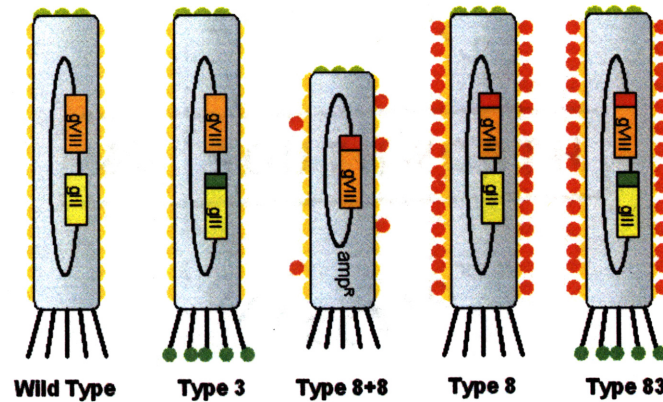


Figure 1. M13 phage display systems. Type 3 or type 8 phage can be obtained by genetically engineering of N-terminal region of gene III (gIII) or gene VIII (gVIII). Type 8+8 phage contains restricted amount of modified pVIII by introducing phagemid with genetically engineered gVIII. For type 83 phage, both gIII and gVIII are modified.

pVIII (approximately 2700 molecules) is major capsid protein, and needed to form the cylinder-like structure which surrounds its single strand DNA (ssDNA). The length of the phage is proportional to the integrated ssDNA during assembly of phage particles, and can be controlled to be about 50 nm by engineering of intergenic region (IR) of phage ssDNA [9]; the IR contain the replication origin ((+) and (-) strands) and packing signal (PS) for integration of the ssDNA to phage particles.

Type 8+8 M13 bacteriophage (Fig. 1) was used as templates for synthesis of inorganic nanowire of metals, semiconductors and magnetic materials [10-12]. The random display of the selected peptide (7-12 amino acids) on pVIII (type 8+8 phage) produces the randomly distribution of inorganic crystals and irregular shape of the nanowire.

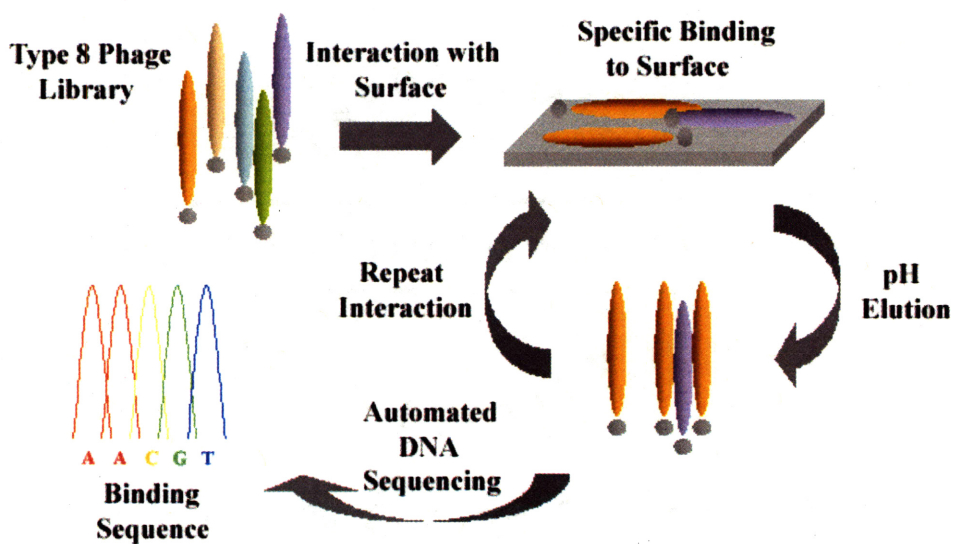


Figure 2. Biopanning with Type 8 phage library. Inorganic target surface is immersed into solution containing type 8 phage library, washed away the excess phage, and eluted using 0.2M Glycine-HCl (pH 2.2). The eluted phage is amplified, and the process is repeated several times to find the tightest binders. The number of plaques can be titered, and each plaques is amplified and sequenced to determine the selected peptide sequence.

An octapeptide type 8 phage display systems has been used for selection to small molecules (dioxin), display of antigenic epitopes (ConA), and selection of chloroform

resistant phage.[13] The distance between the peptides on pVIII is approximately 27Å. However, prior to this work the homogenous peptide display system on pVIII or both pIII and pVIII has not been used as biological scaffold for inorganic materials.

The octamer peptides for inorganics can be selected against inorganic wafer or powder after 4-5 round biopanning in TBST (50 mM Tris-HCl (pH 7.5), 150 mM NaCl, 0.1% (v/v) Tween-20) with pH elution (pH 2.2, 0.2M Glycine-HCl). The sequence of the peptide can be confirmed by sequencing of isolated ssDNA, as illustrated in Figure 2.

1.3. Directional Alignment of Phage Particles.

Rod-like molecules will form liquid crystal (LC) structures depending on their concentration and applied force, such as electrical and fluidic force. The nematic liquid crystalline characterized by uni-directional orientation is often observed in solution of rod-like molecules. The mono-disperse (in length) rod-like molecules provide more preference of smectic phase, in which the rod-like molecules organize themselves into layers roughly perpendicular for the oriented direction of the molecules, than poly-disperse rod-like molecules [14]. The LC phase of the mono-disperse bacteriophage particles are changed by increasing the concentration through nematic, smectic A, and smectic C phase sequentially (Figure 3).[15, 16] The LC phase structures are vary in the phage-based films due to the variation of the concentration during the fabrication by drying; the smectic phase is observed at the edge of the dried film, and the phenomenon can be explained well by the “coffee ring effects”, in which the replenishment from the interior to the edge during the

evaporation of liquid drops causes outward flow and more concentrated materials to the edge than center.[17] In addition, the directional orientation of the rod-like molecules can be obtained by flowing the molecules. The long axis of the rod-like molecules prefers to be parallel to the direction of the flow, and the degree of the directional orientation can be increased by the increase of the flow rate [18]. The genetically engineered type 3 bacteriophage can be used for alignment of its target molecules (inorganic, organic, and biological nanosized molecules) by forming the smectic LC phase.[19]

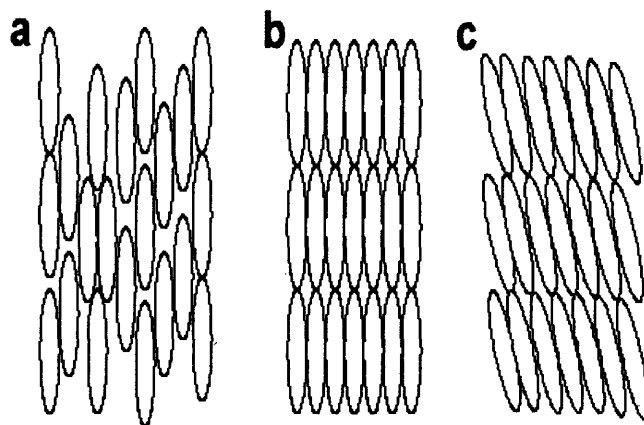


Figure 3. Liquid crystal phases of phage. (a) nematic, (b) smectic A, and (c) smectic C phase, where the axis of the rod-like molecules are tilted.

1.4. Three Dimensional Self-Assembly of Biological Molecules.

The biological molecules, especially peptides, have been used as building block for self-assembly due to their biological characteristics such as ligand recognition,

biocompatibility, and biodegradability. For example, the pH dependent interaction of the helical peptides were used as a dendrimer scaffold [20] and cross-linker for reversible hydrogels [21, 22], which is a network of hydrophilic polymers with water as dispersion medium. The proper intramolecular folding of the peptides affects the peptide interaction and supramolecular structures [23]. The environment (pH, Temperature, light, and ligands) sensitive hydrogels with biological or non-biological copolymers has been studied due to their potential in various application such as biosensors, drug delivery, and bioseparation [24]. Temperature dependent solubility and pH dependent ionization condition of the copolymers affect the hydrogel structure (swelling-shrinking transitions). In addition, the hydrogel by combination of antibody and antigen immobilized polymer chains was reported to response the free antigen reversibly [25]. However, the synthesis of the desire peptides using automated Fmoc solid phase peptide synthesis and recombinant DNA techniques require a lot of cost and effort. The filamentous bacteriophage can be amplified easily by infection to its host, *E. coli*, and the desired peptide can be displayed on their coat proteins, pVIII and pIII. Therefore, self-assembly of type 8 or type 83 phage can be eligible and applicable for fabrication of bio-inorganic hybrid materials.

1.5. Sol-Gel Method for TiO₂ Particle and Phage Stability.

Several chemical methods were introduced to make ceramic nanoparticle synthesis, including reverse micelles method, low-temperature wet-chemical synthesis with a salt precursor, and Sol-gel technique.[26-29] The role of the sol-gel processing has been

growing rapidly in hybrid organic-inorganic materials [30]. The process commonly used for fabrication of metal oxides via the colloidal particle (sol, 1 nm - 1 μ m), through the hydrolysis of the metal alkoxides and condensation in alcoholic solution, and gelation of the sols. TiO₂ is the most widely studied material by the process with titanium alkoxides, such as titanium(IV) ethoxide (Ti(OC₂H₅)₄). Size and shape controls of TiO₂ have been obtained successfully by sol-gel method with chemical additives.[27-29] Rate of the hydrolysis is important, and the slower hydrolysis typically leads to more unique properties. For this reason, the sols are produced in alcoholic solution, and the choice of the solvents is important; higher alkoxy group size lead to decrease of the hydrolysis due to steric hindrance [31]. The sol-gel processing in reverse microemulsion was used for the size controlled inorganic nanoparticles, and its crystallization by drying and calcination [32]. These harsh conditions lead to limitation for biological applications. Natural polypeptide from diatom cell walls, which contain controlled production of nano-structured silica, has been used to catalyze the formation of silica at neutral pH without alcohols [33] and to encapsulate enzyme in the biomimetic silica support [34]. The shape controls of silica using the synthetic block copolypeptides was reported [35]. However, the phage-displayed peptide library has not been used to select peptide for shape controls.

The infectivity of filamentous phage particles is related to the stability of the assembled pVIII molecules and the conformational change of the pIII sub-domains. Although phage particles demonstrate great chemical [36] and thermal [37] stability, certain organic solvents cause morphological change from chloroform and dissolution of the phage from alcohols. Type 8 phage library has been used to select chloroform resistant phage[38].

However, the infectivity in alcohols is inversely dependent upon alcohol hydrophobicity. Phage particles are not stable in approximately 60% of ethanol (30min, 20°C), and the infectivity is not changed in the pH range of 5.0-9.0 [39].

Due to the harsh condition of the general sol-gel synthesis, the phage-displayed peptide library could not be used to select peptide which can bind to precipitated inorganics during this synthesis. Therefore, it is worth studying a new method to select a peptide for inorganics in non-aqueous solution using the type 3 phage library which can survive in the non-aqueous solution.

1.6. Background on Inorganic Nano-materials.

The controlled size of inorganic materials can lead to different chemical and physical properties in nanoscopic dimensions (quantum confinement effects), and the nanoscales materials show intermediate behavior between that of bulk material and molecules.

In semiconductor crystals, the change of the size affects bandgap which is the energy to excite an electron from the valence band to the conduction band, and the excitation involves a loosely bound electron-hole pair known as excitons. Exciton Bohr radius, or the size of an exciton in a bulk crystal, is used to estimate the dimension for the quantum-confinement effects in semiconductor materials. When the size of the semiconductor nanocrystals approaches the exciton Bohr radius, the effective bandgap is increased, and blue-shift of optical transition is observed. The range of the exciton Bohr radii are from 2.2 nm (ZnS) to 7.5 nm (CdTe) in II-VI semiconductors, and from 11 nm

(InP) to 60 nm(InSb) in III-V semiconductors [31, 40]. The exciton Bohr radius of bulk CdSe is 5.6 nm. In addition, the bandgap variation can also be affected by the shape of semiconductor crystals [41]. The bandgap of rod-shaped crystals was known to be decreased with increasing length/diameter ratio [40, 41].

In magnetic materials, the size of magnetic domain usually decreases to minimize the total effective magnetic moment in macroscopic magnetic materials, and energy requirement for domain wall formation limits the decrease of domain size. This infers that the nanoparticles which are smaller than the minimum domain size have single-domain. Due to higher coercivity in single-domain than multi-domain, the coercivity is dependent on the size of particles. The minimum domain sizes are known to range from 10 to 100 nm. If the size of a ferromagnetic nanoparticle is too small (1-10 nm), the particle exhibits a behavior similar to paramagnetism at temperature below Curie temperature [31, 42].

In ceramics, acid-base reactions on metal oxide surfaces have been known to be potentially applicable as catalysts for a variety of important chemical reactions. Several oxides (including MgO, CaO, Al₂O₃, SiO₂ and ZnO) have been used in chemical applications due to their properties to absorb a variety of organic molecules. Also, photocatalytic effects of TiO₂ have been known and widely studied.[26] Because of the high surface area to volume ratio of nanoscale materials, ceramic nanomaterials should have great reactivity on their surface, and their properties can be chemically applicable for catalysts.

CHAPTER 2: Cobalt Ions Mediated Self-Assembly of Genetically Engineered Bacteriophage for Biomimetic Co-Pt Hybrid Materials

2.1. Abstract

Biological scaffolds are used for the synthesis of inorganic materials due to their ability to self-assemble and nucleate crystal formation. We report the self-assembly of engineered M13 bacteriophage as template for Co-Pt crystals. An M13 phage library with an octapeptide library on the major coat protein (pVIII) was used for selection of binders to cobalt ions. Fibrous structures with directionally ordered M13 phage were obtained by interaction with cobalt ions. Co-Pt alloys were synthesized on the fibrous scaffold, and their magnetic properties were characterized. The mineralization showed organized nanoparticles on fibrous bundles. This approach using the phage pVIII library allows for genetic selection that both induces assembly of the phage and directs mineralization of the selected inorganic material.

2.2. Introduction

Precise recognition and self-assembly are required for the proper structure and function of biological components. Due to their ability to interact with high specificity on the nanoscale level, biological molecules are potential building blocks for 'bottom up' fabrication of supramolecular architectures. In nature, matrices of biological macromolecules form mechanical frameworks in biomineralization systems, such as collagen (bone),[43, 44] silicatein (silica sponges),[45, 46] cellulose (plant silica), β -chitin (crab cuticle, mollusk-shells),[47, 48] and lustrin A (mollusk-shells).[49] However, the use of biological macromolecules for biomineralization in vitro is more limited due to the ability to synthesis and purify the complex macromolecules required for the controlled synthesis of the material.

Peptides that have specificity for inorganic compounds have been selected using peptide libraries,[6] and used successfully for the nucleation and growth control of the inorganic nanoparticles in aqueous solution at room temperature.[7, 8] Filamentous bacteriophage (f1, fd, and M13) are excellent biological building blocks due to their controllable length and ability to display multiple peptides. The wild-type filamentous bacteriophage is approximately 930 nm in length and 6 nm in diameter. The phage surface consists of five capsid proteins (pIII, pVI, pVII, pVIII, and pIX). The pIII protein is expressed in five copies at the end of the phage, and is commonly used to display foreign molecules, such as natural peptides, random peptides, proteins, and protein domains. The major coat protein, pVIII, is expressed in 2700 copies per phage and forms the cylindrical

structure that surrounds the viral single stranded DNA (ssDNA). Type 8 phage display systems have been introduced, in which the pVIII proteins have been modified to display selected octapeptides. The peptides are displayed at distances approximately 2.7 nanometers from one another and have included antigenic epitopes (ConA), peptide that specifically bind to small molecules (dioxin), and those that confer chloroform resistance.[13] The homogenous type 8 phage have defined lengths and could be used as genetically programmed biological scaffolds for inorganic materials.

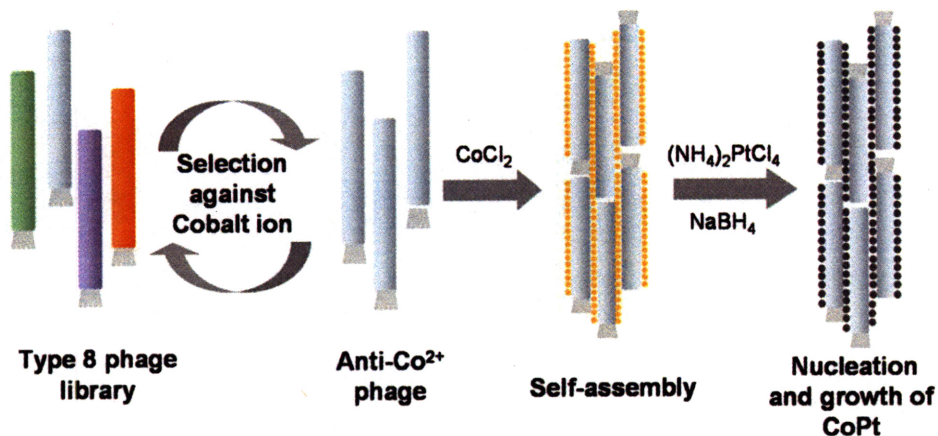


Figure 4. A schematic diagram illustrating formation of Co-Pt hybrid material using a self-assembled phage framework (orange dots = cobalt ions, black dots = Co-Pt).

Nanophase Co-Pt alloys have been studied extensively in the past as a magnetic material, due to the high magnetocrystalline anisotropy, $\sim 5 \times 10^7$ ergs/cm³ for face-

centered tetragonal (fct) phase. Here, we used the genetically engineered type 8 phage library to select phage that displayed peptides with affinity for the cobalt ion. The selected type 8 phage were then used to form the biological mechanical framework for a bio-inorganic (CoPt) hybrid material by cobalt ion mediated self-assembly (Figure 4).

2.3. Materials and Methods

2.3.1. Materials. All chemicals were obtained from Sigma Aldrich unless otherwise noted. M13KE phage vector, *Pst* I, *Bam*H I, and Klenow fragment (3'→ 5' exo⁻) were purchased from New England Biolabs (NEB). Oligonucleotides were from Integrated DNA Technologies. XL1-Blue Electroporation Competent Cells was obtained from Stratagene. Chelating Sepharose Fast Flow gel was purchased from Amersham Biosciences. 2-40% TBE polyacrylamide gel was from Invitrogen. dNTP was purchased from Promega. Tris buffered saline (TBS) solution (pH 7.5) was prepared in house from NaCl (Mallinckodt Chemicals) and Tris base (Roche).

2.3.2. Type 8 phage library. The M13KE phage vector was modified by making a cloning site for pVIII display (Appendix A). A *Pst* I restriction site was made by mutating T to A at position 1372, a *Bam*H I site was made by mutating C to G at position 1381, and the *Pst* I site at position 6246 was deleted by mutating T to A at position 6250. The site-directed mutagenesis was done using overlap extension PCR. A dsDNA library was then prepared and cloned into the resulting modified phage vector, named M13SK, using *Pst* I and *Bam*H I. To obtain the dsDNA library, partial library duplexes were formed by annealing of

extension primer (5'- GATGCTGTCTTTTCGCTGCAG-3') with oligonucleotides (3'-ACGACAGAAAGCGA CGTCnm(nnm)₆nnCCTAGGAACATC ATC-5', where n = A, T, C, or G and m = A or C). The partial library duplexes were incubated with Klenow fragment (3'→ 5' exo⁻) (10 U/μl) and dNTP at 37°C for 30min. The Klenow fragment was inactivated by heating (75°C for 20 minutes), and the mixture was digested with *Pst* I and *Bam*H I. The digested DNA was gel purified (2-40% TBE polyacrylamide gel), ligated into M13SK, and transfected to XL1-Blue Electroporation Competent Cells using a MicroPulser™ (Biorad) (Figure 5). The library was titered according to manufacturer directions and sequenced (MIT Biopolymers Laboratory) before amplification.

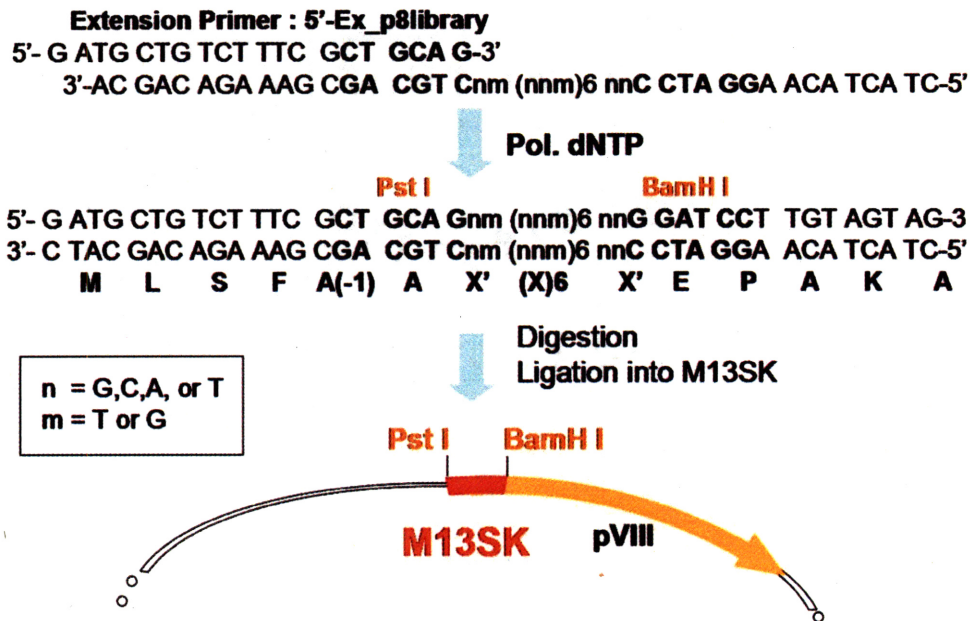


Figure 5. Scheme for construction of type 8 phage library in M13SK. Schematic shows the restriction sites for cloning DNA library into M13SK. X = any randomized amino acids.

2.3.3. Biopanning against Co ion. The selection of type 8 phage with affinity towards Co^{2+} was performed by incubating the type 8 phage library ($\sim 10^{10}$ pfu) with Co^{2+} immobilized on 200 μl of Chelating Sepharose Fast Flow gel in TBS buffer (pH 7.5) with 0.15% tween-20. The bound phage were washed 10 times with the incubation buffer and then eluted with 50mM histidine. The fourth elution was amplified for the next round of biopanning. After the fourth round, the eluted phage was amplified, and the sequence was conformed.

2.3.4. Synthesis of Co-Pt on phage templates. The anti- Co^{2+} phage (1×10^8 pfu/ μl) was incubated with 3.75 mM cobalt(II) chloride hexahydrate ($\text{CoCl}_2 \cdot 6\text{H}_2\text{O}$) in TBS buffer (pH 7.5) for 30 min. The mixture was then incubated with ammonium tetrachloroplatinate ($(\text{NH}_4)_2\text{PtCl}_4$, 1.25 mM final concentration) at room temperature for 30 minutes before being reduced with sodium borohydride (NaBH_4 , 1.25 mM final concentration).

2.3.5. Characterization. Polarized optical microscopy (Olympus) was used for optical microscopy and cross-polarized optical microscopy (CPOM) images. Transmission electron microscopy (TEM) and high-resolution TEM (HRTEM) images were obtained using JEOL 200CX and JEOL 2010 TEMs (JEOL), respectively, at an accelerating voltage of 200 kV. Energy dispersive spectroscopy (EDS) and chemical element mapping data were taken using an HB603 Scanning TEM (STEM) at 250 kV. Scanning electron microscopy (SEM) images were obtained using a JEOL 6320FV field-emission SEM at 1kV after dialysis, freeze-drying, and gold sputter coating. Magnetic properties were characterized using a DC super conducting quantum interference device magnetometer (DC SQUID) (Quantum

Design). The effective magnetic anisotropy energy density (K_{eff}) can be estimated by Neel's theory,[50]

$$25k_B T_B = K_{eff} V, \quad (1)$$

where k_B is the Boltzmann constant and V is an average volume of particles. The true magnetic moment at a particular temperature above T_B was calculated by fitting the magnetization curve (Figure 4c) to the Langevin function,[51, 52]

$$M = M_s \left(\coth \left(\frac{\mu H}{k_B T} \right) - \frac{k_B T}{\mu H} \right), \quad (2)$$

where μ is the true magnetic moment of each nanoparticle, M_s is the saturation magnetization, T is the absolute temperature, and H is the applied magnetic field.

2.4. Results and Discussion

After four rounds of biopanning against Co^{2+} using the type 8 phage library, a dominant Co^{2+} binding phage displaying the octapeptide, EPGHDAMP, was selected. The peptide sequence contained a well known metal binding motif, EXXH, which can be found within active sites of metalloproteins, an especially diverse class of diiron proteins. The active sites consist of four-helix bundle coordinated by metal ions.[53, 54]

There are some metal-binding motifs which coordinate well for high affinity to metal cations, including zinc-finger motifs. High content of the metal binding amino acids (D, E, H, and C) could be expected. However, the preference of amino acids in the type 8 phage library was tested by comparing the observed percent of each amino acid to expected percent ((number of DNA codons for an amino acid / total number of DNA codons) \times 100) from sequence analysis of 50 randomly chosen clones (Table 1). Cysteine and lysine residues in the library were not observed, and basic amino acids are not preferable compared to acidic amino acids. That may due to preference of basic amino acids at C-terminal and acidic amino acids at N-terminal of pVIII proteins for electrostatic stability.² The aromatic residues (Phe, Tyr, and Trp) were not observed frequently, compared to the expected value. The library shows higher percentage of glycine and proline, which have effects on the flexibility and the conformation of peptide backbone. The bias is presumably due to the compatibility of electrostatic and structural change with phage major coat protein assembly. For rational design, we tried to display EEEEE, CCCCC, or HHHHH at N-terminal of pVIII, but the repeated amino acid sequence were not compatible for phage assembly and stability. For this reason, the selected peptide sequence using type 8 phage library could satisfy both the affinity to Co^{2+} and the structural compatibility to pVIII proteins.

Table 1. Percentage of amino acids in type 8 phage library

Amino acids	Observed %	Expected %
Arg, Lys, His	3.2	15.6
Asp, Glu	15.4	6.3
Ser, Thr	21.5	15.6
Ala, Val, Leu, Ile	23.6	25.0
Gln, Asn	5.3	9.4
Phe, Tyr, Trp	3.3	9.4
Gly, Pro	24.8	12.5

* Expected percent = (number of DNA codons for an amino acid / total number of DNA codons) \times 100

The selected type 8 phage, named anti-Co²⁺, was used for Co²⁺ mediated self-assembly of phage. CoCl₂ (3.75 mM in TBS pH 7.5) was incubated with 1×10^8 pfu/ μ l anti-Co²⁺ or wild-type (M13KE) phage. Phage bundles were observed in the sample containing the anti-Co²⁺ phage after 30 min (Figure 6a, center) but were absent in the samples containing wild-type phage (left) and no phage (right). CPOM revealed birefringence in the phage bundle (Figure 6d) indicating the bundle formation with directional order. A transmission electron micrograph of the bundles positively stained with uranyl acetate (1%) showed a sponge-like texture (Figure 6c), in which the direction of bundle is parallel to the long axis of the phage particles. The directional order of the rod-like molecules has been shown to be dependent on their concentration and the force applied.[55] In these experiments, the addition of cobalt ions stimulated the formation of bundles with directional ordering at phage concentrations much lower ($\sim 10^8$ pfu/ μ l) than that required for liquid

crystalline (LC) formation ($\sim 10^{12}$ pfu/ μl).^[19] The directional ordering could be due to increased local concentration of phage and induced interactions between phage particles.

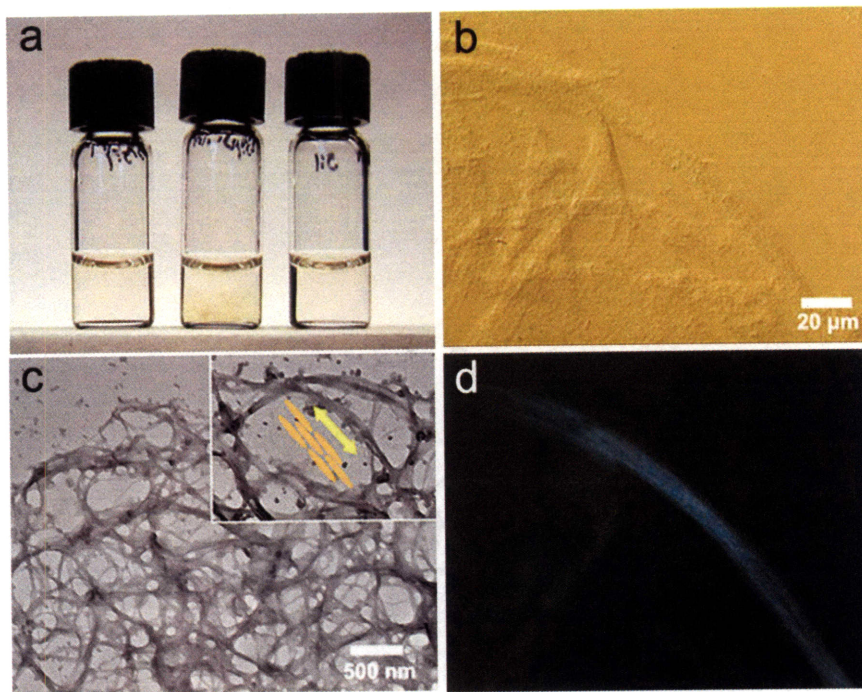


Figure 6. (a) Photograph of cobalt mediated fibrils in solution using wild-type (left), anti- Co^{2+} (center), and no phage (right). (b) Optical microscopy image and (c) TEM image of the fibrils (from center sample). Inset: directional placement of phage particle along the bundle (d) Cross-POM image of (b).

Co-Pt nanoparticles were then synthesized on the phage bundles by adding $(\text{NH}_4)_2\text{PtCl}_4$ to the solutions and reducing them with NaBH_4 . Mineralization of Co-Pt was observed on the darkened fibrous networks of anti- Co^{2+} phage (Figure 7a, center) but not in the solutions containing wild-type phage (left) and no phage (right). Aggregated Co-Pt was

observed without phage (Figure 8a). Wild-type phage did not form the fibrous structure in the presence of cobalt ions (Figure 8b), and an aggregate of black precipitation was observed in the vial. The presence of Co and Pt was confirmed by using EDS. Structures with the composition ($\text{Co}_{0.35}\text{Pt}_{0.65}$) were observed with anti- Co^{2+} phage, whereas structures with composition ($\text{Co}_{0.25}\text{Pt}_{0.75}$) were observed with wild-type or no phage. The difference could be due to different local concentration of cobalt near surface of the phage particles. The hybrid $\text{Co}_{0.35}\text{Pt}_{0.65}$ phage material was dialyzed and freeze-dried, and its micro-scale texture was examined by SEM (Figure 7b). Crystal growth on the oriented phage fibrils was characterized by using TEM (Figure 7c, d). The stripe patterns observed on the bundles are ~ 6 nm in width, close to the diameter of a phage particle. The selected area electron diffraction (SAED) pattern shows the fundamental ring pattern of fcc CoPt.[56] A HRTEM image (Figure 7e) shows the lattice fringe of the nanoparticles, indicating their crystalline nature. The lattice spacing of the crystal is ~ 0.214 nm, which is in good agreement with the estimated values of 0.219 nm for [111] facet of fcc $\text{Co}_{0.35}\text{Pt}_{0.65}$ by Vegard's law.[57] The average particle size from the HRTEM is 2.3 nm (SD = 0.23 nm) (Figure 7f).

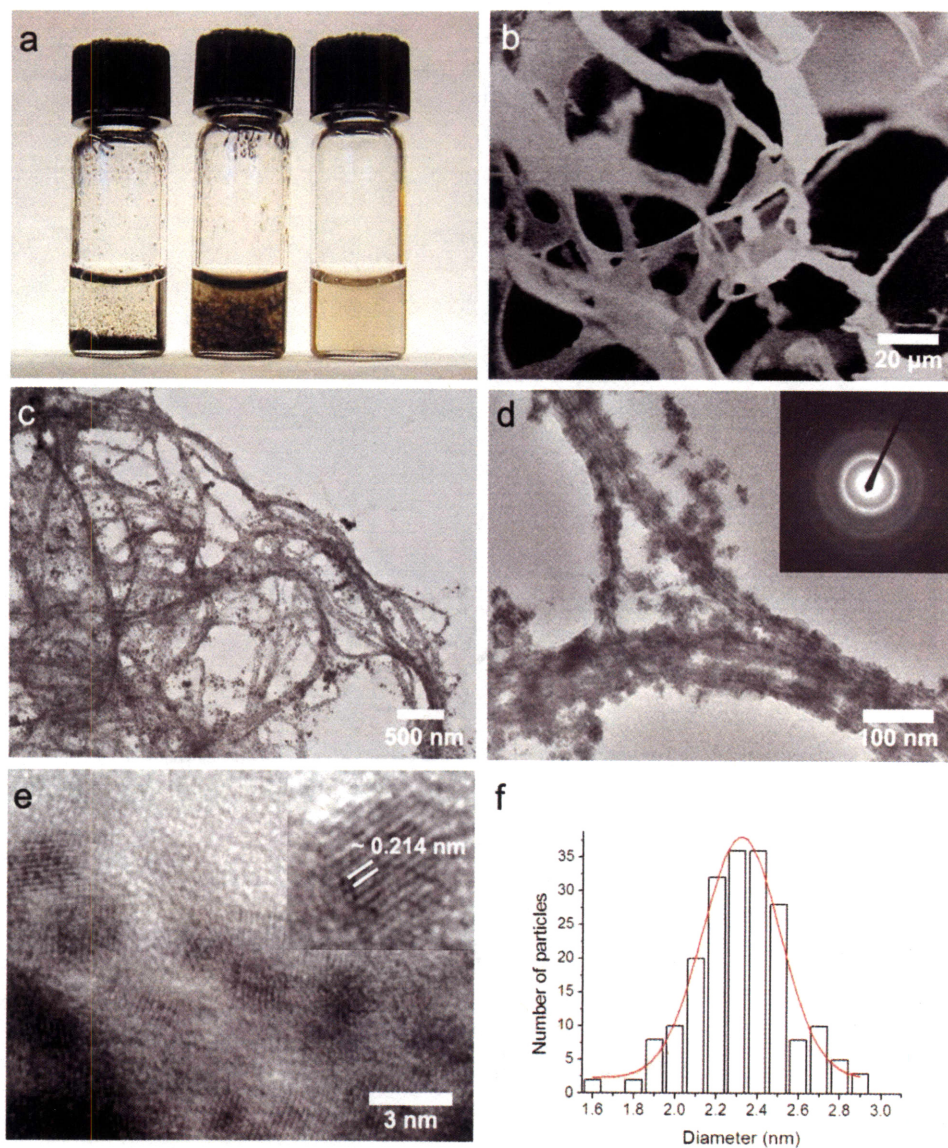


Figure 7. Synthesis of Co-Pt nanoparticles on fibrous phage template. (a) Solution after nucleation and growth of Co-Pt with wild-type (left), anti-Co²⁺ (center), and no phage (right). (b) SEM image of the anti-Co²⁺ sample after freeze-drying. (c) TEM image of the anti-Co²⁺ sample. (d) TEM image showing bundled phage. Inset: SAED pattern of Co-Pt. (e) HRTEM of individual Co-Pt nanoparticles showing lattice fringes and a lattice spacing (inset). (f) Distribution of particle diameters from TEM images (average particle size = 2.3 nm).

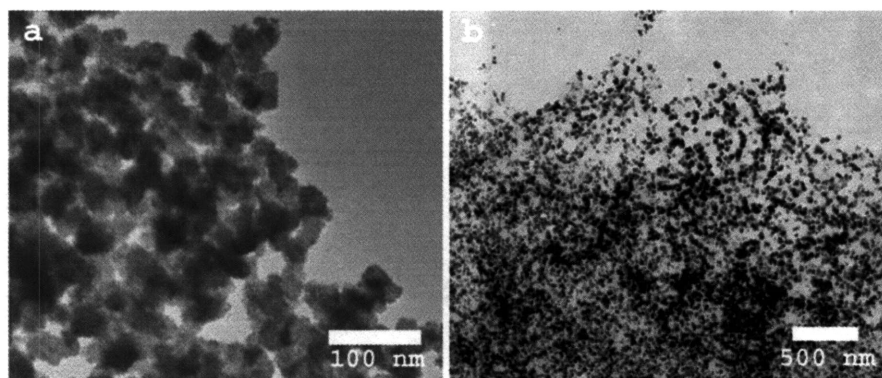


Figure 8. TEM image of Co-Pt without phage (a) and with wild-type phage (b).

M13 bacteriophage with partial peptide display on pVIII (type 8+8 phage) have previously been used as templates for synthesizing inorganic nanowires of semiconductors[58] and magnetic materials.[11, 59] The random display of the selected peptide (7-12 amino acids) on pVIII in these reports produces the random variable in packing density of modified pVIII coat proteins along the phage and makes it difficult to always obtain identical structure. Unlike the type 8+8 systems, we obtained clearly defined inorganic placement on phage particles in the bundle structure. Individual phage with $\text{Co}_{0.35}\text{Pt}_{0.65}$ nanoparticles can be visualized with regular thickness of the inorganic layer.

STEM and EDS mapping were used for the chemical analysis of the $\text{Co}_{0.35}\text{Pt}_{0.65}$ hybrid material. Consistent atomic ratios of Co-Pt was observed (Figure 9a), showing regular composition along the fibrous phage template. Elemental mapping of Co and Pt

(Figure 9b, c) on a fibrous phage template suggested that the nanocrystals on the template are alloys of Co and Pt.

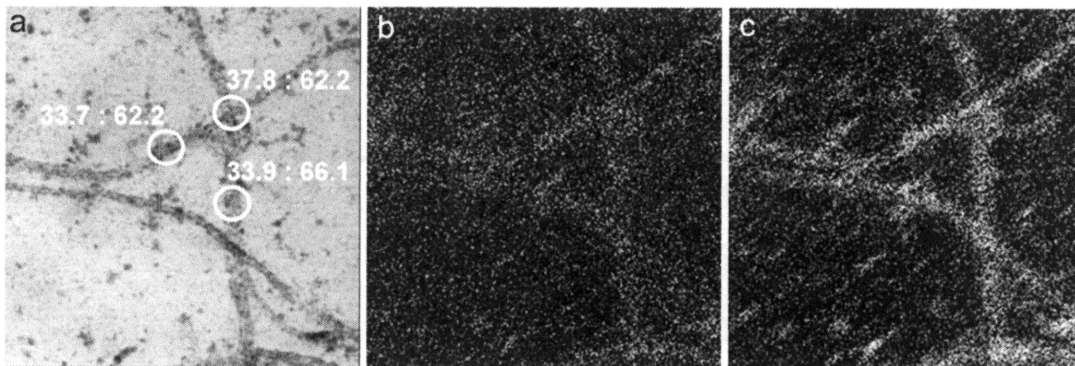


Figure 9. (a) STEM image of Co-Pt nanoparticles prepared on the fibrous phage bundle. Atomic ratios of Co and Pt on fibrous structure are shown. (b) Co and (c) Pt map showing distribution of Co and Pt.

The magnetic properties of the hybrid material were measured with DC SQUID. The zero-field-cooling (ZFC) and field-cooling (FC) magnetization (M) were monitored as a function of temperature (Figure 10). The ZFC mode was carried out by cooling to 5 K in a zero field and then heated up to 300 K in a 100 Oe field. Field cooling magnetization was achieved by cooling to 5 K and heating up to 300 K in the present of a 100 Oe field. The observed blocking temperature (T_B), which is the characteristic temperature with maximum ZFC magnetization, was 50 K. Typical superparamagnetic behavior of single domain nanoparticles was observed, showing divergence of the ZFC and FC curves below T_B and coincidence of the curves over T_B . From the measured T_B and average particle size, the estimated K_{eff} is 2.7×10^7 ergs/cm³ which is high compared to the value for fcc Co_{0.35}Pt_{0.65}

film ($\sim 7 \times 10^6$ ergs/cm³) [60] and close to the value for the ordered fct phase of CoPt ($\sim 5 \times 10^7$ ergs/cm³). The high K_{eff} can be explained by surface effects on magnetic anisotropy. [61] Based on a report of size-dependent magnetic properties of cobalt nanoparticles that showed a decrease of T_B by increasing of cobalt nanoparticle size, the diameter of cobalt nanoparticles would be expected to be ~ 6 nm when the T_B is 50. [26] The estimated particle size is not in agreement with our measured data (~ 2.3 nm) using TEM. Therefore, I believe the hybrid material is not a mixture of cobalt nanoparticles and platinum nanoparticles, but an alloy.

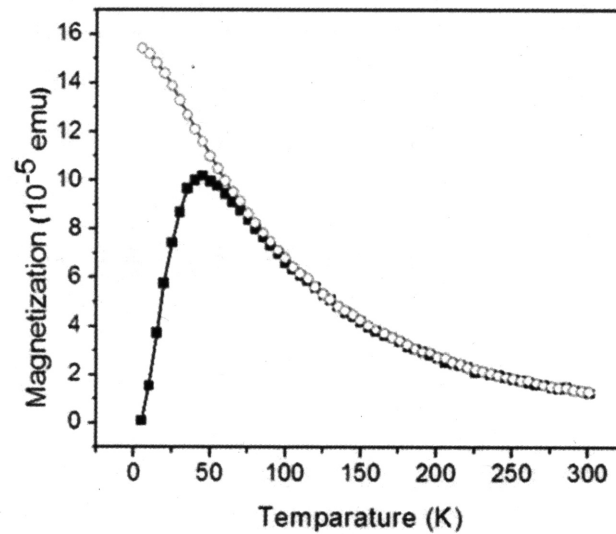


Figure 10. ZFC (solid rectangle) and FC (open circle) magnetization as a function of temperature. Sample was cooled with (FC) or without (ZFC) magnetic field (100 Oe) to 5K, and then heated up to 300K.

In addition, typical superparamagnetic behavior was observed from field dependent magnetization at 5K and 300K (Figure 11). Coercivity and remanence were zero above T_B , whereas an asymmetric hysteretic feature was observed below T_B (coercivity ≈ 782 Oe), suggesting the presence of the exchange anisotropy, which is observed at the interface of ferromagnetic and antiferromagnetic materials.[62] Thus, it is possible that an antiferromagnetic oxide layer could be present. We also believe that the interaction between the nanoparticles and the phage matrix can contribute to the asymmetric hysteresis behavior. The magnetization curve at 300K was well fitted to the Langevin function (Figure 12). The magnetic moment per CoPt particles was calculated to be $4008 \mu_B$ (Bohr magneton).

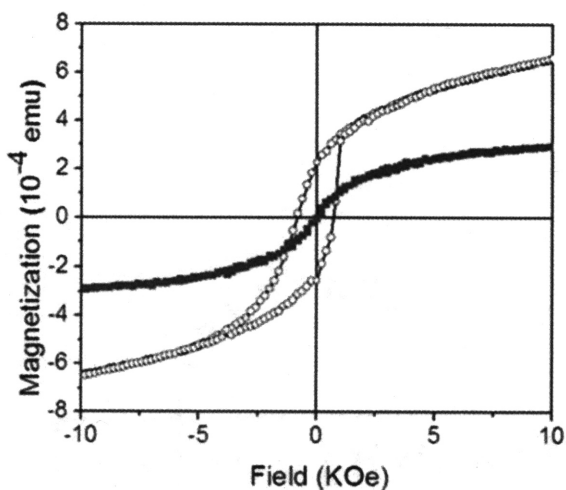


Figure 11. Magnetization versus applied magnetic field at 5K (solid rectangle) and 300K (open circle).

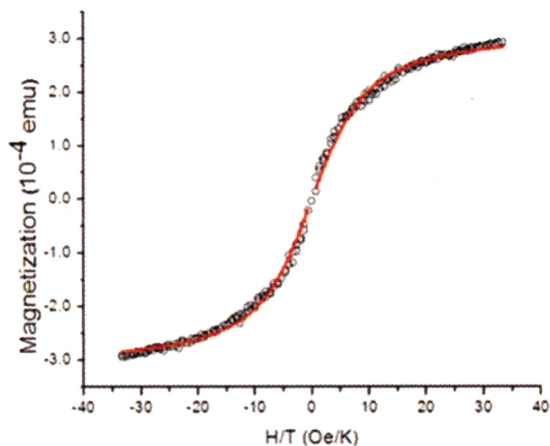


Figure 12. Fit for the Langevin function at 300K (red line).

2.5. Conclusions

In this chapter, I have described the selection of genetically modified type 8 phage particles having affinity to a metal ion and the metal-ion mediated bundle formation of these particles at low phage concentrations. The sponge-like morphology of phage bundles was used as a template to nucleate Co-Pt nanoparticles which are both regularly located on the phage structure and show a narrow size distribution. The hybrid material showed typical superparamagnetic properties with high anisotropy. We believe that the introduced method can be used for other inorganic materials, such as metals and semiconductors. The further modification of the pVIII display library to include modified gene III and gene IX will allow for additional peptides to be displayed on the phage capsid to simultaneously organize multiple types of inorganic materials.

CHAPTER 3: Phage Displayed Peptide Selection for TiO₂ in a Non-Biological Environment.

3.1. Abstract

Peptide assisted mineralization in mild conditions has been utilized to impose morphological and size control of inorganic nano-crystals. Herein, I introduce an *in vitro* molecular selection method in non-biological conditions for inorganic synthesis. A phage display peptide library which is resistant to ethanol was constructed and used for selection against titania in 90% ethanol. The selected peptide, with a conserved basic amino acid sequence, promotes nanoparticles (~ 60 nm) during titania synthesis by the traditional sol-gel method. This *de novo* method could be applicable for bio-mineralization in other non-biological conditions.

3.2. Introduction

Biological macromolecules, such as proteins and polysaccharides, are known to control the morphology of inorganic crystals. This control is imposed by limitation of spatial boundaries and inhibition of crystal growth at particular crystal planes, at which metal binding active sites have a preferred structural arrangement to the ordered metal ions.[63] Peptides for inorganic recognition have been successfully selected using peptide display technology [6, 64] and have been used for biomimetic synthesis and assembly of inorganic nanoparticles.[65] Bacteriophage, E-coli, and yeast peptide display systems have been introduced for the *in vitro* evolutionary methods in physiological environments.[66] However, the systems can not be used in non-biological conditions due to cellular stress and structural instabilities.

The synthesis of inorganic nanoparticles in non-aqueous solution by the sol-gel technique is the preferred and widely used method for metal oxide synthesis. The role of sol-gel processing has grown rapidly in hybrid organic-inorganic materials [67]. The process commonly used for fabrication of metal oxides is the hydrolysis of metal alkoxides and condensation in alcoholic solution via the colloidal particle. The rate of the reaction process is an important parameter in determining the properties of the final product, and can be controlled by the choice of solvent.[26] Sol-gel processing through reverse microemulsion was introduced for size controlled inorganic oxide nanoparticles and crystallization by drying and calcinations. [32] These harsh conditions lead to a distinct limitation for biological applications.

The morphological control of silica has been studied using natural polypeptides from diatom cell walls [33, 34] as well as synthetic block copolypeptides [35] at neutral pH. Biological systems including proteins [68] and fungus [69] have also been used for titania synthesis in mild conditions. However, phage-displayed peptide library has not been used to select peptides for growth controls in non-biological environments.

The infectivity of filamentous phage particles is related to the stability of the assembled pVIII major coat proteins and the conformational change of the pIII sub-domains. Although phage particles demonstrate great chemical [36] and thermal [37] stability, filamentous bacteriophage is not stable in non-aqueous solvents for extended periods of time. For example, chloroform is known to cause morphological changes in phage particles. [38] A type 8 phage library, which contains random peptides at the N-terminal of the pVIII coat proteins, has been used to select chloroform resistant phage. The increased stability could be due to the altered surface properties created by displaying peptides on the exterior of phage. [38] Also, phage particles are known to be unstable in approximately 60% ethanol (30 min, 20°C). The infectivity in alcohols is inversely dependent upon alcohol hydrophobicity and is not affected by pH in a range of 5.0-9.0. [39]

For peptide assisted growth control of inorganics in non-aqueous solution, the peptide should be selected in the solution that will be used for inorganic synthesis. Due to the harsh conditions of the general sol-gel synthesis, the phage-displayed peptide library could not be used to select peptides which can bind to the surfaces of inorganics. We introduce a new method for peptide selection against inorganics using the type 3 phage library which can survive in non-biological solvents. TiO₂ was used as an example due to

the type 8 library was incubated in 90% ethanol (19% TBS, pH = 7.5) for 20 min at room temperature, and survived phage was amplified for 4.5 hours before next round of selection. After third round of the selection, the survived phage was titered, and sequence of peptide was confirmed (MIT Biopolymers Laboratory).

3.3.2. Infectivity assay in ethanol. $\sim 2 \times 10^{10}$ pfu/ml of ethanol resistant phage and wild-type phage in 0.1 ml of 50%, 70%, and 90% ethanol was incubated for 10, 20, 30 min and 1 hour. At the end of incubations, the samples were diluted 100-fold with TBS in order to stop the incubation and ensure proper titering. The concentration of phage solution was confirmed by following general titering methods.

3.3.3. Ethanol resistant pIII phage library. To make the pIII library of the surviving type 8 phage, the library oligonucleotide 3'-GGGCCCATGGAAAGATAAGAG TGAGA(NNM)₈CCACCACCAAGCCGGCTTTGTAC-5' was annealed with the extension primer (5'-CATGCCCGGGT ACCTTTCTATTCTC-3'), and the extended duplex was obtained by incubation of the annealing reaction with Klenow fragment (10 U/ μ l). N is one of four bases and M is one of A and C. The duplex and dsDNA of the surviving type 8 phage was digested with *Acc65 I* and *Eag I*, and ligated after gel-purification (8% nondenaturing polyacrylamide gel and 1% agarose gel respectively) (Figure 14). The library was titered, after transfection into XL1-Blue Electroporation Competent Cells using a MicroPulser (Biorad). The complexity of the pIII library was $10^8 \sim 10^9$ pfu from the titering.

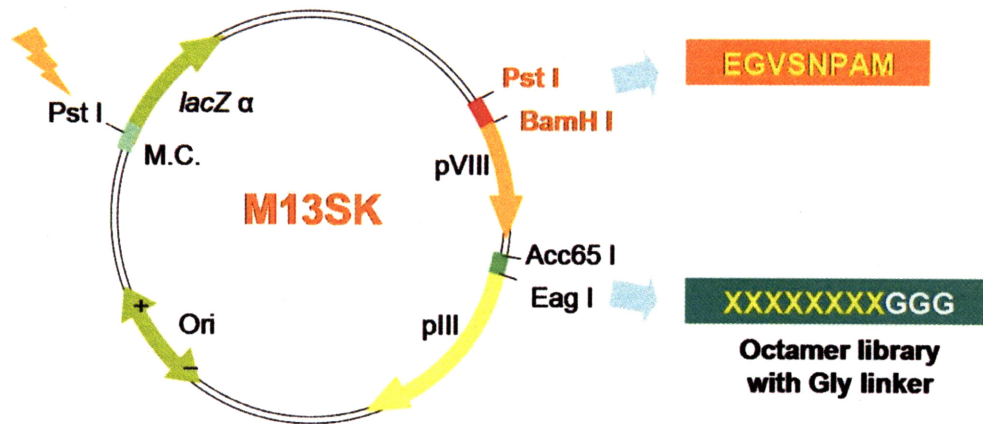


Figure 14. Scheme for construction of ethanol resistant pIII phage library. dsDNA of ethanol resistant phage with “EGVSNPAM” insert at N-terminal of pVIII are modified to have octamer peptide library with Gly-Gly-Gly linker at N-terminal of pIII. (X = random amino acids)

3.3.4. Biopanning against TiO₂. The phage displayed pIII library was incubated with a TiO₂ wafer (rutile, 110) (Wafer World Inc.) in 90% ethanol (10% TBS, pH = 7.5). To elute the bound phage, the solution was boiled with 100 µl of Tri buffer (pH = 8) for 10 minutes, and the ssDNA of the phage was isolated. The pIII and pVIII regions of the isolated ssDNA was amplified by using PCR with primers 5'-M13SK-1351 (5'-GATGCTGTCTTTCGCTGCA-3') and 3'-M13KE-2 (5'-GACAGGAGGTTGAGGCAG-3') (length of PCR product = 926 base pairs). The amplified region was used to

make new pIII library by digestion with *Pst* I and *Eag* I, ligation and transfection. After the fourth round of the selection, the selected peptide sequence was determined.

3.3.5. Synthesis of TiO₂ with the selected peptide. Titanium(IV) ethoxide (Ti(OC₂H₅)₄) (Aldrich) in ethanol was added to 90% ethanol (10% TBS, pH = 7.5) with and without K1 peptide, which was chemically synthesized (MIT Biopolymers Laboratory). The final concentration of peptide and Ti were about 50 μM. The mixtures were incubated at room temperature for 24 hours.

3.3.6. Characterization. Transmission electron microscopy (TEM) and high resolution TEM (HRTEM) images were obtained using JEOL 2000FX and JEOL 2010 TEMs (JEOL) respectively at an accelerating voltage of 200 kV. Element line-scanning was taken using JEOL 2010FX TEM in scanning mode. Scanning electron microscopy (SEM) images was obtained using a JEOL 6320FV field-emission SEM at 1kV after Au coating (50Å thickness). X-ray photoelectron spectroscopy (XPS) spectra were recorded using a Kratos AXIS Ultra System (MIT, center of material science and engineering) with monochromatized AlK α radiation at 150 W. Samples were prepared by drying TiO₂ particles on gold substrates. Electron binding energies were calibrated using gold 4f (84.00 eV) as a reference. Passing energy for survey and high-resolution spectra were 160 and 10 eV respectively. CasaXPS software was used for curve fitting. Peak areas were divided by the corresponding elemental sensitivity factor [72] to calculate atomic ratio.

3.4. Results and discussion

Phage which can survive in ethanol were selected after three rounds of biopanning in 90% ethanol. Characterization of the displayed peptides reveal a predominant sequence (36/49) with conserved Glu, Asn, and Met amino acids, which can act as hydrogen bonding donors or acceptors (Figure 15a). Pro and Gly in the sequences could affect structural flexibility for increased stability of phage particles. The first amino acid in the pVIII peptide library can be 5 amino acid (Ala, Val, Asp, Glu, and Gly), and Glutamic acid are preferred in wild-type phage. It is possible that the first Glutamic acid could be due to intrinsic preference. However, when sequences of the pVIII library were tested by sequencing of 41 phage plaques, the first amino acid were Ala (nineteen), Val (five), Asp (two), Glu (five), Gly (ten). Therefore, I could not exclude a possible contribution of Glu for structural stability in 90% ethanol.

Structural stability was studied indirectly by monitoring changes of infectivity in a series of ethanol concentrations and incubation times (Figure 15b). Both wild type and the selected phage showed conserved infectivity during incubation in 50% ethanol for 1 hours. The infectivity of wild-type phage was decreased rapidly in 70% ethanol, and no phage particles were observed after incubation in 90% ethanol for 10 min. The infectivity of wild-type phage agreed with a previous phage stability study.[39] Ethanol resistant phage showed similar infectivity in both 70% and 90% ethanol. 100-fold decreases were observed after 20 min incubation in 90% ethanol. The ethanol resistant phage showed much higher stability than wild-type, and the phage is applicable for ethanol resistant pIII phage library.

a

36	E	G	V	S	N	P	A	M
1	E	G	P	P	N	P	G	M
1	E	E	P	N	T	F	M	P
1	G	A	T	P	N	P	A	M

b

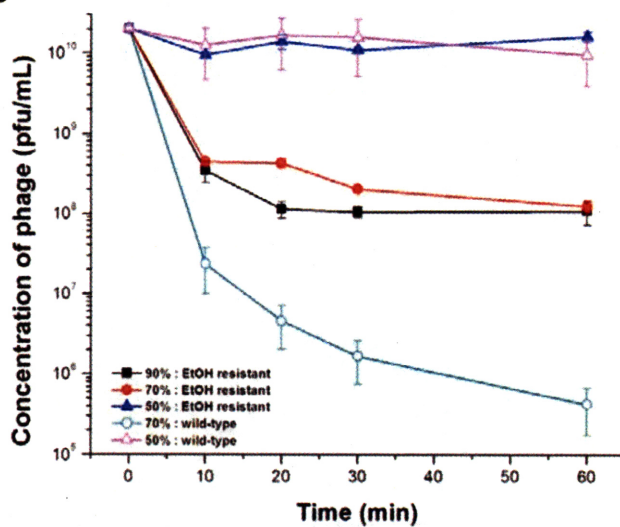


Figure 15. Ethanol resistant phage. (a) pVIII displayed peptide sequences with numbers of observed sequences (left panel), (b) infectivity of predominant resistant phage in series of different time and percent of ethanol.

The pIII phage library in which random octapeptide library with Gly-Gly-Gly linker was constructed using the ethanol resistant phage and used for selection in 90% ethanol against a TiO₂ wafer (110, rutile). After three rounds of biopanning, conserved sequences of peptides were observed with positively charged amino acids (Arg, Lys, and His) (Figure 16). Peptides selected under physiological conditions against metal oxides (SiO₂, ZnO, CaCO₃, Cr₂O₃, and Fe₂O₃) often contain basic amino acids,[65] and electrostatic interactions are believed to be major binding force.[73] Because the dielectric constant of 90% ethanol (10% water) (29.03) is lower than that of water (80.37) at 20 °C,[74] electrostatic interaction in 90% ethanol could 2.77 times stronger than those in water due to their reciprocally proportional relationship.

K5	R	S	V	A	H	M	R	L
K16	H	T	L	P	R	D	K	R
K18	R	G	H	M	Y	T	T	H
K4	R	L	T	I	D	R	T	A
K10	K	S	S	S	Q	R	L	P
K1	M	R	Q	L	E	R	A	S
K19	E	K	T	G	V	R	T	L
K11	E	R	E	R	P	P	R	M
K8	G	A	R	H	Q	P	W	R
K2	V	P	T	R	N	T	I	K

Figure 16. Selected peptide sequence in 90% ethanol against TiO₂ crystal. Conserved basic amino acids (red); Arginine (R), Lysine (K), and Histidine (H). Peptides were named by sequenced order (left panel).

The K1 peptide was used to study the effects of the peptide during hydrolysis and condensation of titanium ethoxide. The TEM image in Figure 17a shows particle formation with about 60 nm, whereas the well controlled individual particles were not observed without the peptide. Figure 18 show that particles without the peptide are various in size and are linked together to become a network which can be observed easily by traditional sol-gel method.[75] Electron diffraction (inset) pattern exhibits rings with d spaces of 3.51, 2.35, and 1.92 Å corresponding to (101), (004), and (200) respectively (anatase phase, JCPDS 21-1272). Lattice images were obtained using HRTEM show that a particle is mixture of amorphous and nanocrystalline TiO₂. of anatase of anatase (Figure 17b). The presences of peptides bound to TiO₂ particles were confirmed by line-scan using STEM (Figure 17c), showing Ti, O, and S elements. The high intensity of O and the presence of S suggest incorporation of peptides in the particles. The particles were washed with 90% ethanol (10% water) and precipitated by centrifugation at 18000 rcf for 10 min. The precipitant was Au coated with 50Å thickness and characterized by SEM (Figure 17d). Particle size determined by SEM agrees with the size determined by TEM.

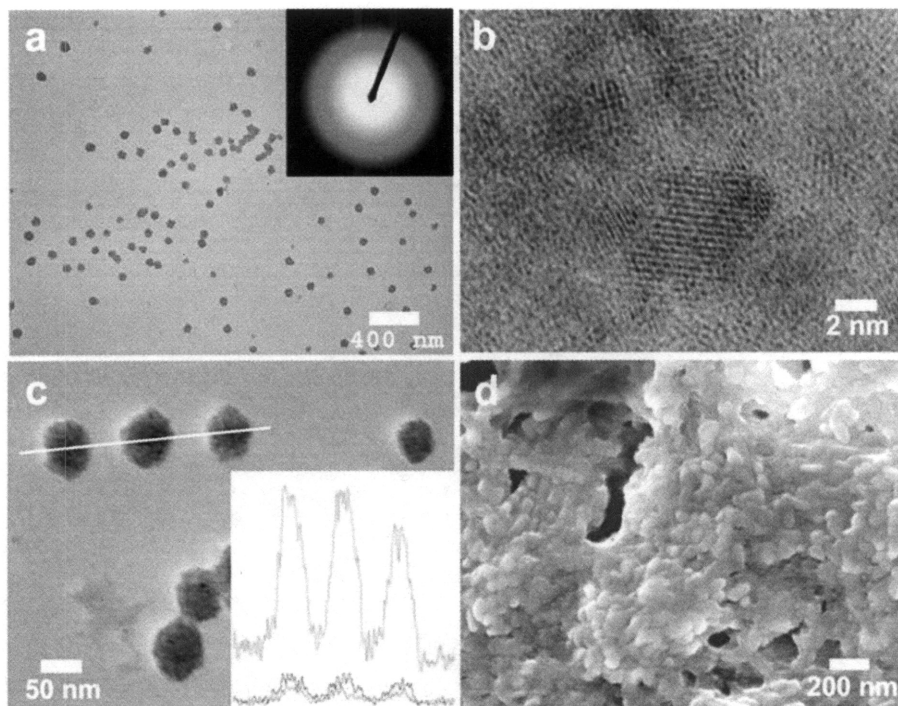


Figure 17. TiO_2 particles with K1 peptide. (a) TEM image with diffraction (inset), (b) HRTEM showing (101) and (004) facets, (c) line-scan using STEM for elements of Ti (red), O (green), S (blue), (d) SEM image of precipitated particles.

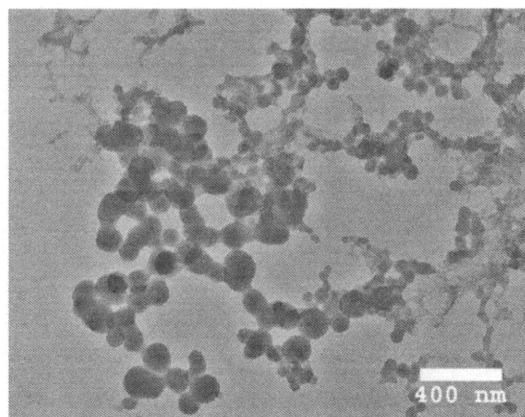


Figure 18. TEM image of TiO_2 without K1 peptide showing irregular particles which is linked together.

Element composition and oxidation states of the particles were analyzed by XPS. A survey of elements (Figure 19) shows the presence of Ti, O, C and N in both the precipitant with and without the peptide, whereas S 2s and 2p peaks were observed only with peptide, supporting that the particles is mixture of TiO_2 and peptide. From high resolution XPS (Figure 20), Ti 2p_{1/2} (458.9 eV) and Ti 2p_{3/2} (464.7 eV) spins with 5.8 peak separation indicate that most Ti are in +4 oxidation state.[76] The peaks were observed in both the sample with and without peptides. The high oxidation states could be due to preference of hydrolysis of $\text{Ti}(\text{OC}_2\text{H}_5)_4$ which is about five orders higher than $\text{Si}(\text{OC}_2\text{H}_5)_4$. [26] High resolution oxygen (1s) spectra for the sample with the K1 peptide (Figure 21a) show three major peaks at 530.4, 532.2, and 533.4 eV attributed to oxygen in metal oxide, surface hydroxyl, and adsorbed water or organic components respectively.[77] These assignments for the sample without the peptide (Figure 20b) were made for oxygen at similar positions (530.6, 531.9, and 533.1 eV). The ratio of oxide oxygen to titanium were near the theoretical value of 2.0 in both samples with and without the peptide (1.90 and 1.88 respectively). The relative amount of surface hydroxyl to titanium was decreased from 4.78 to 2.58 by addition of the peptide, suggesting interaction of oxide with peptide. Electrostatic interaction could contribute to stabilize oxide and reduce the chance for hydroxylation. These results support the preference of basic amino acids in selected peptide against metal oxides.[65] The additional peak at 531.3 (Figure 21a, green) which appeared with K1 is considered to be the amide-O species from the peptide.[78]

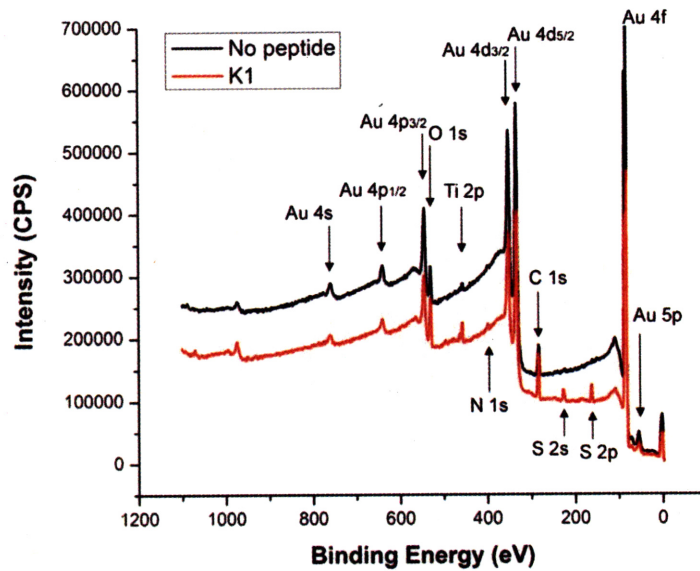


Figure 19. XPS of TiO_2 precipitants. (a) Survey of TiO_2 with and without K1. Additional peaks for N and S were observed in sample with K1 peptide (red line).

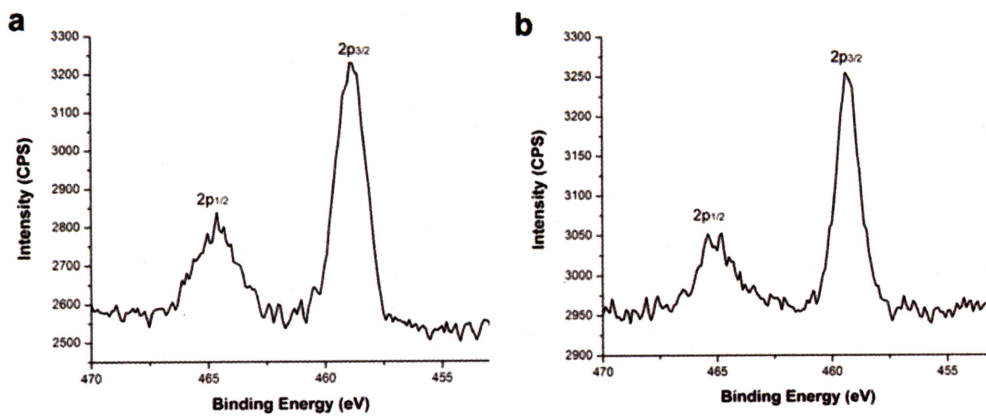


Figure 20. High resolution XPS spectra of Ti 2p peak of TiO_2 with K1 (a) and without K1 (b).

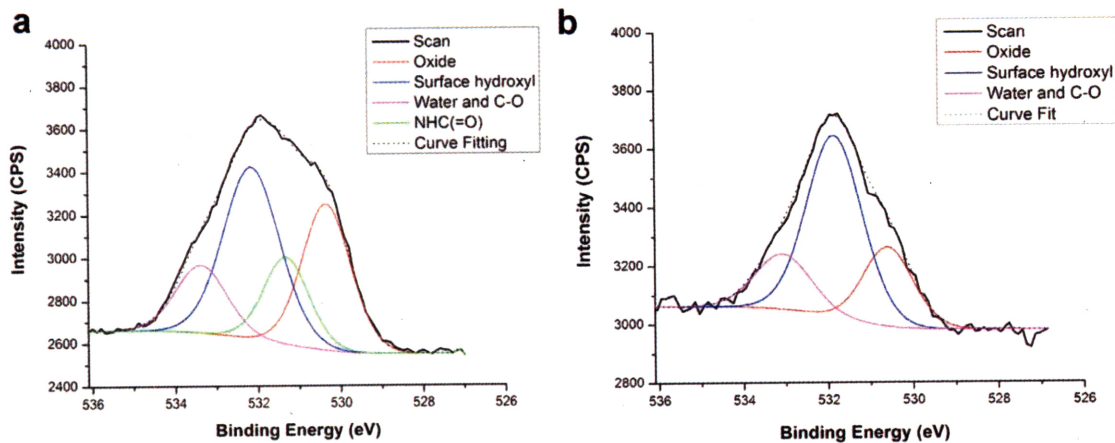


Figure 21. High resolution XPS spectra of Oxygen 1s spectra with K1 (a) and without K1 peptide.

3.5. Conclusion

In this chapter, I describe the selection of ethanol resistant phage using a type 8 phage library and the subsequent construction of a pIII peptide library by genetic engineering of the resistant phage to select a binder to TiO_2 in ethanol environment (90% ethanol). The selected peptide was synthesized and shows to impose morphological control during TiO_2 synthesis. The peptide assisted synthesis results in spherical particles in which interaction of peptide and TiO_2 was observed by XPS. Sol-gel chemistry is widely used for synthesis of oxide materials in alcoholic conditions. This method could have applications in bio-mediated inorganic growth for materials in non-biological solvents.

CHAPTER 4: Alignment and Storage of Biological Molecules in Phage Film.

4.1. Abstract

Filamentous bacteriophage can form liquid crystalline films in high concentration due to their rod-like shape. Here I report the storage of proteins in smectically aligned phage films. β -galactosidase and a green fluorescent protein variant were successfully stored in the phage film with increased stability. In addition, streptavidin conjugated phycoerythrin was aligned in S1 phage films, in which a streptavidin binding peptide is displayed at the end of phage particles. Alignment, with increased fluorescent intensity of phycoerythrin, was achieved. Proteins stored in phage film could have applications in biologically functional materials and biosensors.

4.2. Introduction

In order to maintain their biological activity, enzymes and protein drugs must sustain their three-dimensional structure. Degradation of protein structure occurs easily during dehydration and storage. Carbohydrates, including sucrose, lactose and trehalose, have been extensively studied as excipients for stabilizing membranes, proteins and cells upon dehydration, and are widely used for biological materials in pharmaceutical industry.[79, 80] Long-term storage of proteins in biocompatible and biodegradable polymers is challenging due to their applicable opportunities in the treatment of disease by sustained release. Poly(lactide-co-glycolide)(PLG) is an example of stabilization of a protein by encapsulation. [81]

Filamentous bacteriophage can form well-controlled liquid-crystalline (LC) phases due to their rod-like shape. The self-assembly of nanoparticles in LC phase films of genetically engineered phage has been demonstrated.[15, 16] The phage film could be used for biocompatible functional materials due to their multiple peptide display systems. Here I report a new protein storage method with ordering in phage film.

In order to show enzyme stability in viral films, β -galactosidase was used, which has been widely used as a reporter enzyme. Sucrose/glucose, which has been shown to preserve the structure and function of biological systems during dehydration and subsequent storage, was used to enhance the stability of enzyme. Green fluorescent protein variant (GFPuv) was used to visualize the functional and structural stability of proteins in the viral film. GFPuv is known to emit green light (maximum emission wavelength at 509 nm) when it is in stable structures. Streptavidin conjugated phycoerythrin and anti-streptavidin phage

were used to demonstrate alignment of biological molecules along with their stability (Figure 22).

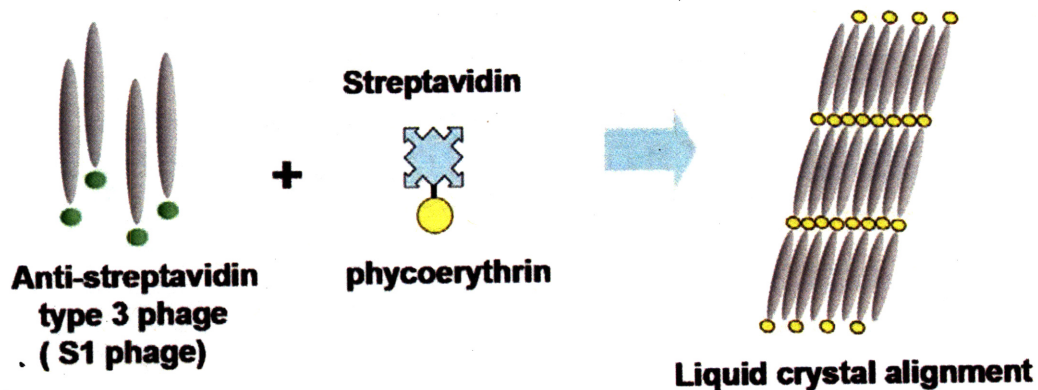


Figure 22. Scheme for alignment of streptavidin conjugated phycoerythrin in smectic phage film. Streptavidin can bind to an end of a phage particle which displays streptavidin binding peptides at N-terminal of pIII.

4.3. Materials and Methods

4.3.1. β -galactosidase stability in phage film

β -galactosidase in phosphate buffered saline (PBS) solution (pH 7.0, concentration: potassium phosphate: 10 mM , NaCl: 0.3 M) was mixed with stock solutions of glucose, sucrose, and M13 phage to the final concentration: 0.5mg/ml β -galactosidase, 5mg/ml glucose, 50mg/ml sucrose, and 1.25mg/ml phage. Aliquots (20 μ l) of the solution were pipetted to 1.5ml Eppendorf tubes, dried in a dessicator for two days, and stored at room temperature in darkness. To measure activity of β -galactosidase, the dried viral films were

suspended in 500 μl of PBS solution (pH 7.0). 100 μl of the suspension and 700 μl of o-nitrophenyl galactoside (ONPG) (1.5×10^{-2} M) were combined in a disposable cuvette. The enzyme activities (units) were obtained by monitoring an increase of absorbance of o-nitrophenol (ONP) at 420nm for 10 min at 30 sec intervals. One unit of activity was defined as the amount of enzyme that can catalyze the transformation of 1 μmol of ONPG into ONP in 1 min at 25°C (pH 7.0).

4.3.2. GFPuv stability in phage film

The DNA encoding GFPuv (Clontech) was amplified by PCR and subcloned into pFLAG-CTC vector (Sigma) for the expression of GFPuv-FLAG in *Escherichia coli*. Whole cell extract was prepared, and the expressed GFPuv-FLAG was purified using an anti-FLAG M2 affinity gel column (Sigma). The mixture of GFPuv-FLAG, phage, and glucose/sucrose (1:10 w/w) was prepared with the final concentration: 100 $\mu\text{g}/\text{ml}$ GFPuv-FLAG, 5 mg/ml phage, and 5 mg/ml glucose, and 50 mg/ml sucrose. 10 μl of the mixture was dispensed on a glass slide, and dried in a desiccator for a day. GFPuv-FLAG stability was visualized by using confocal fluorescence microscopy. Additionally, the dependence of concentration change of glucose/sucrose was monitored at 2.5 and 25 mg/ml respectively.

4.3.2. Alignment and stability of phycoerythrin in phage film

To fabricate phage films with aligned phycoerythrin, as an example biological molecule, 200 μl of the Anti-streptavidin type 3 phage (S1 phage) suspension ($\sim 6 \text{ mg mL}^{-1}$, 1.9×10^{-7} M in Tris-HCl saline buffered solution (pH 7.5) was mixed with 200 μl of 0.05

mg mL⁻¹ (1.7×10^{-7} M in Tris-HCl saline buffered solution (pH 7.5), 5% (w/v) sucrose, 0.5% (w/v) glucose) of R-phycoerythrin-streptavidin (MW: 292,800) (Molecular Probes). The mixture (400 μ L) in 0.6 mL microcentrifuge tube was dried in a desiccator for two weeks to make bulk phage film. 1 μ L of the mixture was cast and dried on the glass substrate for cast film fabrication. The bulk and cast film textures were studied with POM and confocal fluorescence microscopy (Leica SP2 AOBS). The molar and weight concentration of phage suspensions were measured using a UV-vis spectrophotometer (extinction coefficient: 1.2×10^8 M⁻¹cm⁻¹ at 268 nm). Fluoimager (Amersham Pharmacia) was used to analyze fluorescent intensity of the cast film.

4.4. Results and discussion

The recovered activities of β -galactosidase in the viral film with glucose/sucrose during storage at room temperature were much more preserved than without the carbohydrates (Figure 23). The activities of control samples which were dried in a desiccator without phage and carbohydrates, were dramatically decreased. The phage and glucose/sucrose did not affect the enzyme activity in the suspension before the drying of the film or after suspending the viral film using PBS solution. No significant difference was observed for β -galactosidase activities between freeze-dried and air-dried samples in a desiccator during storage at room temperature.

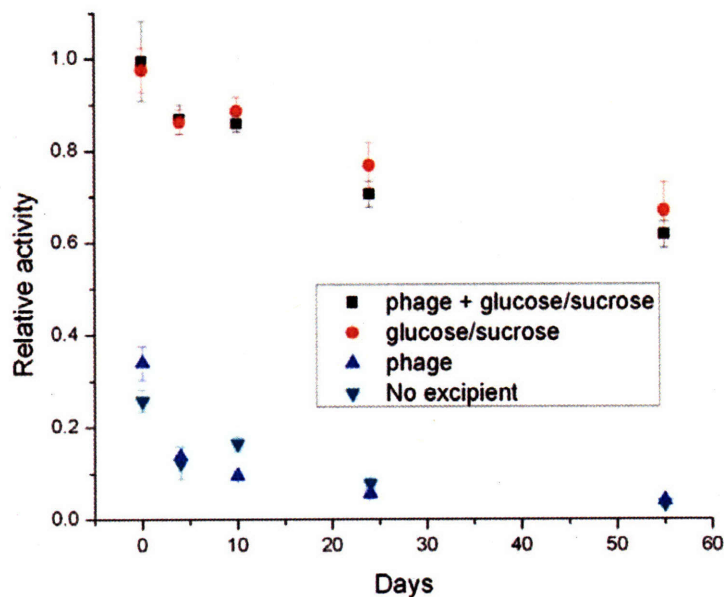


Figure 23. Effect of glucose/sucrose and phage on β -galactosidase activity during storage at room temperature. Day 0 represents the recovered activity after drying in desiccator.

Confocal fluorescent microscopy of GFPuv images showed that GFPuv proteins in the viral film were still active so as to emit the green fluorescent light, when excited at 361 nm. The result showed that the addition of glucose and sucrose helped to form more homogeneous viral films as well as to avoid deformation of the film structure during the film fabrication process. The strong fluorescent image of GFPuv (Figure 24a) indicated that the structure and function of the GFPuv were stored in tact after the complete evaporation of the solvent. Deformation of the film was clearly observed with low or without content of glucose / sucrose (Figure 24b and c). The protein stability in phage films is mostly dependant on glucose / sucrose content.

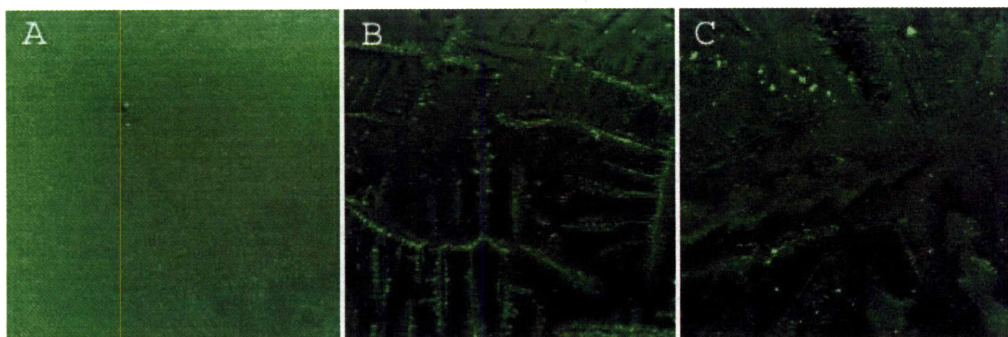


Figure 24. Confocal microscopy images of fluorescent GFPuv in the viral film after one day from their fabrication with same GFPuv and phage concentration and with variation of concentration of glucose / sucrose; (A) 5mg/ml / 50mg/ml, (B) 2.5mg/ml / 25mg/ml, and (C) without glucose and sucrose.

To prepare smectic ordered phycoerythrin-phage film, anti-streptavidin M13 phage ($\sim 6 \text{ mg mL}^{-1}$, $1.9 \times 10^{-7} \text{ M}$ in TBS pH 7.5), streptavidin conjugated phycoerythrin ($1.7 \times 10^{-7} \text{ M}$ in TBS pH 7.5), and sucrose (5%, w/v) were mixed in microcentrifuge tube (0.5 mL), and the suspension was dried in a dessicator for two weeks. The fabricated film is slightly pink in color (emission of phycoerythrin at 578 nm) and transparent (Figure 25a). The optical characterization using POM revealed a $\sim 5 \text{ }\mu\text{m}$ dark-gray periodic horizontal striped patterns (Figure 25b), and the bright and dark patterns are switched depending on the angle between polarizer and analyzer. The uniform equidistant line pattern is caused by chiral smectic C order [82]. The fluorescence properties of phycoerythrin are observed using fluorescence microscopy (Figure 25c), suggesting stable structure of phycoerythrin during fabrication of the film. One micrometer fluorescent striped patterns, which corresponds to

the length of phage ($\sim 1 \mu\text{m}$), were observed using confocal fluorescence microscopy, and the clear striped patterns confirms proper binding of streptavidin conjugated phycoerythrin to the end of the phage (pIII) (Figure 25d).

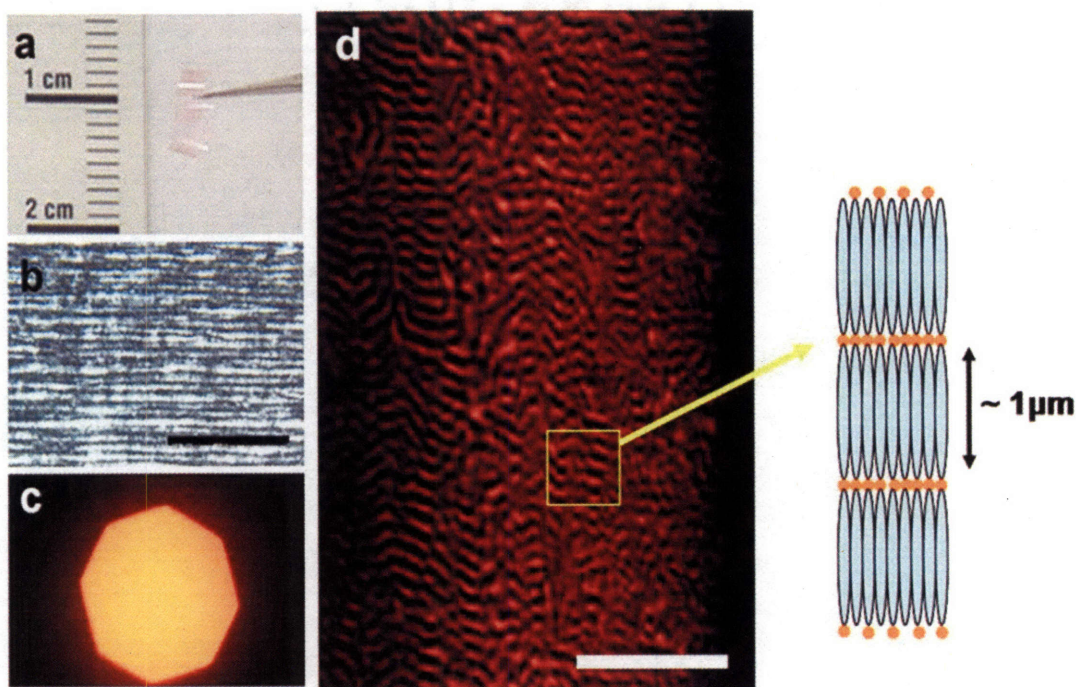


Figure 25. (a) Photograph of phycoerythrin-phage film, (b) POM image of phycoerythrin-phage film (scale bar: $100 \mu\text{m}$), (c) fluorescence image of phycoerythrin-phage film, and (d) phycoerythrin-phage film on glass slide, showing one micrometer striped patterns (scale bar: $10 \mu\text{m}$)

Fluorescence intensity of the phycoerythrin was measured by using fluorimeter to study protein stability indirectly (Figure 26). The fluorescence intensity decreased after drying in a desiccator without glucose/sucrose. Alignment of phycoerythrin with S1 phage

prevents degradation of phycoerythrin during the drying process, but not during long term storage. The carbohydrates conserve about 40% of aligned phycoerythrin activity in the phage film during long periods of storage times. Most biological structures will collapse under air-drying conditions due to surface tension forces. It may possible that the alignment in LC phase of S1 phage reduce a chance of exposure to water and air interfaces.

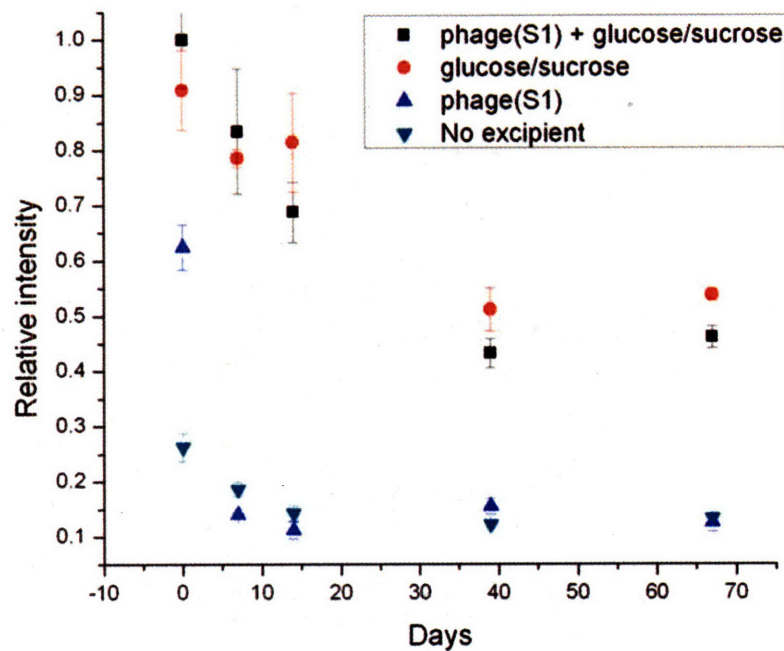


Figure 26. Effect of glucose/sucrose and phage on aligned phycoerythrin during storage at room temperature. Day 0 represents the recovered activity after drying in desiccator.

4.5. Conclusion

The protein stability in the phage film was enhanced with the glucose/sucrose as a stabilizer, compared to that of the phage film without the stabilizers. Randomly dispersed β -galactosidase and GFPuv were successfully stored in wild-type phage film with functional and structural stability. Phycoerythrin was aligned and stored within smectically ordered S1 phage. The alignment could reduce degradation of protein during the drying process. Because the surfaces of phage particles can be modified by displaying desired peptides, the phage film could be applicable for biologically functional materials and biosensors.

The dried phage film fabrication method could be used generally to store other proteins or enzymes with little change of their functions and structures. Furthermore, other stabilizers (such as glycerol and polyethylene glycol)[83] are expected to improve the enzyme stability in viral films.

CHAPTER 5: Assembly of Inorganic Nanoparticles using Genetically Engineered Bacteriophage

5.1. Abstract

Bacteriophage can be potential biological building blocks and templates for alignment and self-assembly of biological and inorganic molecules, because their surface can be genetically engineered to display foreign peptides. Here, pIII and pVIII coat proteins of phage particles were engineered, and their applicability as a nano-structural scaffold were studied. A gold binding peptide was selected by using a type 8 phage library. Self-assembly of gold particles on phage was observed. In addition, type 83 phage which display both streptavidin binding peptide at pIII and Au binding peptide at pVIII were constructed for multiple self-assembly of streptavidin conjugated nanoparticles and Au nanoparticles in two-dimensional architectures. Genetically engineered phage could be applied to ordering complex bio-inorganic nanomaterials.

5.2. Introduction

Biological molecules such as DNA and peptide have been targetted for bottom-up self-assembly of nanoscale structures, which require precise and specific interaction for their right placement. Peptides displayed on bacteria, tobaccomosaic virus (TMV), the cowpea chlorotic mottle virus (CCMV), and the cowpea mosaic virus, have been used for synthesis and self-assembly of inorganic nanoparticles.[84] M13 bacteriophage, a filamentous bacteriophage, is a potential biological building bock for self-assembly of inorganic nanoparticles, because their major coat proteins (pIII, pVIII, and pIX) can be genetically engineered to display desired peptides.

M13 bacteriophage consists of ~2700 copies of pVIII for their cylindrical body, and 5 copies of pIII and pIX are placed at each end of the bacteriophage. Type 3 phage libraries which display peptides at the N-terminal of the pIII protein is the most widely used system to select a binder to biological and inorganic molecules. The selection against inorganic surfaces was successfully demonstrated for peptide mediated inorganic synthesis and growth controls.[6, 8]. Also, Type 8+8 phage systems, in which peptides are displayed partially at N-terminal of pVIII proteins, have been used for inorganic nano wire synthesis.[11] In this system, infection of helper phage in bacteria which contain an engineered phagemid is required. It is hard to obtain mono-disperse phage particles in length, because the length of phage is dependent on the packed DNA sized during assembly of phage particles on the bacterial membrane.

A type 8 phage system, which displays octamer peptides at the N-terminal of all pVIII proteins was introduced for selection against proteins and small molecules.[13] Unlike the phagemid systems, the advantage of this system is that we can get homogenous display on the pVIII resulting in the nucleation of inorganic crystals with uniform placement as well as defined length and width. In addition to engineering the pVIII, the pIII can be completely modified (type 83 system) (Figure 1).

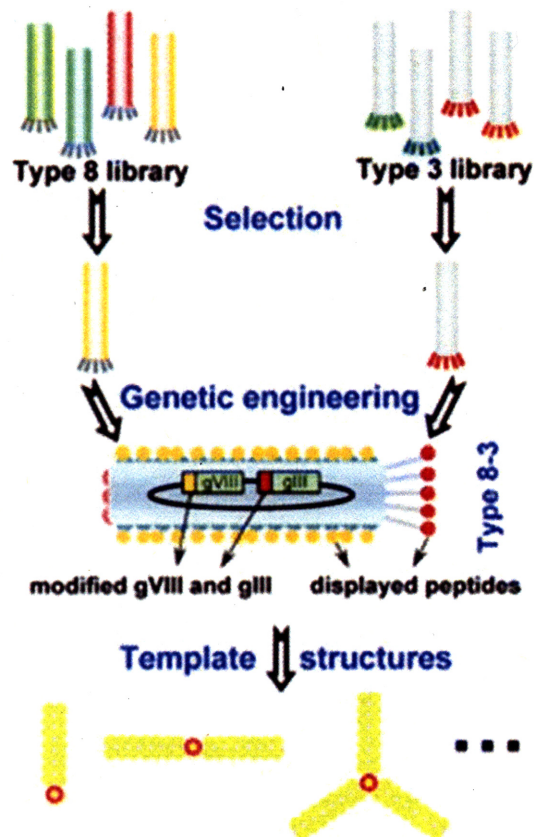


Figure 27. Scheme for the type 83 phage for assembly of Au nanoparticle on pVIII and streptavidin conjugated CdSe nanoparticles on pIII.

The research objective of this chapter is to apply engineered type 8 and type 83 bacteriophage display systems as a biological scaffold for assembly of both Au and CdSe nanoparticles. Type 8 phage and type 3 phage were used for selection against Au and streptavidin respectively, and Type 83 phage which display peptides both pVIII for Au and pIII for streptavidin were constructed for assembly of both Au nanoparticles and streptavidin conjugated CdSe nanoparticles (Figure 27).

5.3. Materials and methods

5.3.1. Biopanning against Au surface by collaboration with Chung-Yi Chiang

A type 8 phage library was constructed as described in chapter 2. The library was incubated in TBST (TBS, pH = 7.7 + (v/v) Tween-20) on a Au surface and unbound phage were washed off. Au binders were eluted by incubation in 100 μ l of 0.2 M Glycine-HCl (pH = 2.2), and the solution was neutralized with 150 μ l of 1M Tris-HCl (pH= 9.1). The eluted phage was amplified for the next round of biopanning. After the fourth round of biopanning, the sequences of the selected phage from randomly chosen plaques were determined

5.3.2. pIII modification of p8#9 phage

To combine the type 8 phage and type 3 streptavidin binding phage, the region from position 1358 to 2277 of the engineered M13KE vector, which contains the streptavidin

binding peptide (WDPYSHLLQHPQ), was amplified using PCR with primer 5'-M13KEmu-p8 (5'-CTGTCTTTCGCTGCAGAGGGTGAGGATCCCGCAAAGC-3') and 3'-M13KE-2 (5'-CACCGTTCATCTGTCTC-3'). The PCR product includes mutation sites (underline parts of 5'-M13KEmu-p8) to generate *Pst* I and *Bam*H I restriction sites for pVIII cloning. The PCR products were digested with Bam H I and Eag I, and ligated into isolated dsDNA of p8#9 phage. The N-terminal pIII and pVIII sequences of the type 83 phage, named #9S1 phage, were confirmed. Details about construction of type 83 phage are described in appendix B.

5.3.3. Assembly of Au nanoparticles on p8#9 phage by collaboration with Chung-Yi Chiang and Yu Huang

10 μ l of p8#9 phage ($\sim 10^8$ pfu/ μ l) were mixed with 100 μ l of Au nanoparticle (5 nm) suspension (5.0×10^{13} particles/mL, Ted Pella). After 2-3 minutes of incubation, TEM samples were prepared. Wild-type phage (M13KE) and p8#17 phage (a minor peptide selected from the type 8 library) were used as control. After uranyl-acetate-staining (1% uranyl-acetate), the control phage were observed by TEM.

5.3.4. Fabrication of nano-architectures by collaboration with Chung-Yi Chiang and Yu Huang

10 μ l of #9S1 phage (10^9 pfu/ μ l) were mixed with 5 μ l of streptavidin conjugated Au nanoparticles (15 nm) and 70 μ l of TBST with 0.1% bovine serum albumin (BSA, Amersham Biosciences). The mixture was agitated for about 1 hour for

binding of the S1 peptide and streptavidin. Then, 10 μ l of the mixture was incubated with 100 μ l of Au nanoparticle suspension (Ted Pella) for binding of Au nanoparticles to the pVIII of #9S1. In addition, streptavidin conjugated Au nanoparticles were replaced with streptavidin conjugated CdSe quantum dot (15 nm) (Quantum Dot) for hetero-nanoparticle structures.

5.4. Results and discussion

After the fourth round of biopanning against the Au surface with the type 8 phage library, the prevalent phage (19 of 20 randomly chosen clones), which is named p8#9, contains the serine rich peptide sequence, Val-Ser-Gly-Ser-Ser-Pro-Asp-Ser (VSGSSPDS). The selected serine rich sequence is similar to other previously selected Au-binding peptides in which serine and threonine are prevalent [85]. Formation of Au wires by incubation of Au nanoparticles (\sim 5 nm) with p8#9 phage was observed using TEM.

The suspension of Au nanoparticles with control phage (wild-type and p8#17 phage) remained clear, as did the suspension of Au nanoparticles without phage (blank control sample) (Figure 28a). The mixture of p8#9 phage and Au nanoparticles result in precipitation (high-lighted by the arrow). Au nanoparticles in the blank control and control phage samples were randomly dispersed (Figure 28b-c). Any regular placement of Au nanoparticles on control phage was not observed (Figure 28c and d), whereas Au nanoparticle on p8#9 phage were assembled and densely packed (Figure 28e). The 1 μ m length and 10 nm thickness are consistent with the size of the M13 bacteriophage. The

enlarged image (inset of Figure 28e) shows alignment of Au nanoparticles on a phage particle, forming a wire-like structure.

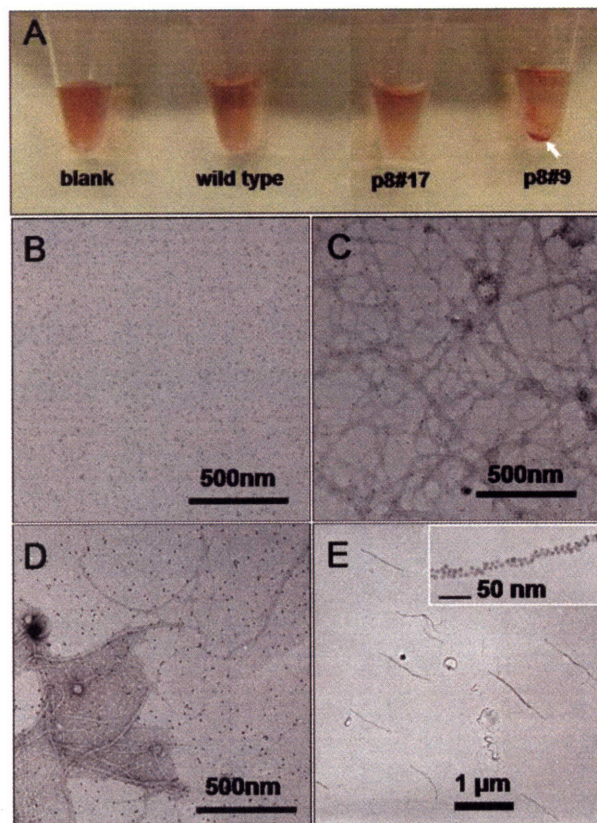


Figure 28. (a) the suspension of Au nanoparticles with and without phage. Blank control sample contains Au nanoparticles alone, and wild-type and p8#17 phage are used as control. p8#9 phage is the selected Au binding phage. TEM image of blank control sample (b), wild-type (c), p8#17 (d), and p8#9 (e) phage. Wild-type and p8#17 phage were stained by using uranyl-acetate (1%).

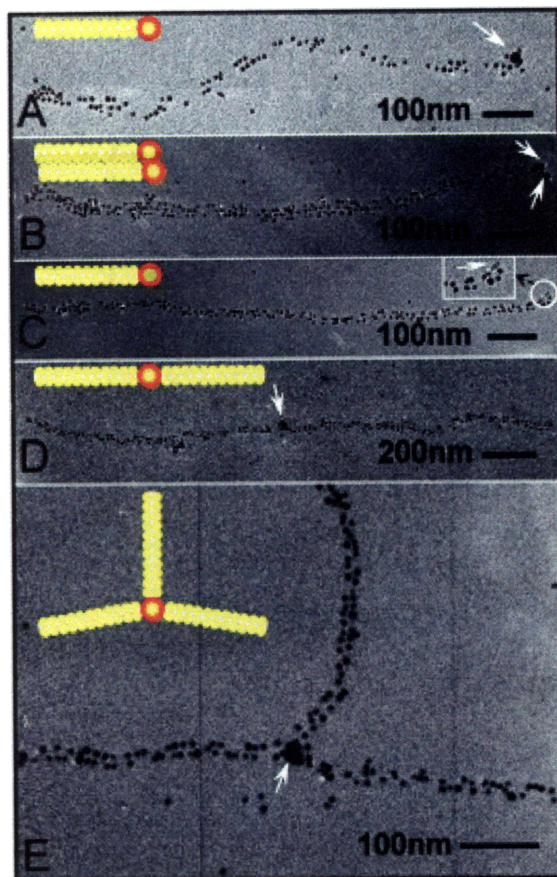


Figure 29. TEM images of various nanoarchitectures templated by #9S1 phage. (a and b) Assembly of Au nanoparticles (5 nm) at pVIII and streptavidin conjugated Au nanoparticles (15 nm) at pIII. (c) CdSe quantum dot (15 nm) at pIII and Au nanoparticles at pVIII. (d and e) example of complex structure in which streptavidin conjugated Au nanoparticle (15 nm) are bridge two or three phage particles.

Streptavidin-conjugated Au nanoparticles (15 nm) and Au nanoparticles (5 nm) were incubated with #9S1, which display both Au binding peptide at pVIII and streptavidin binding peptide at pIII. Specific placement of Au nanoparticles at pIII (15nm Au particles) and pVIII (5 nm Au particles) was observed (Figure 29a and b). Streptavidin conjugated Au

nanoparticles were replaced with streptavidin conjugated CdSe (15 nm) to confirm that this novel method can be extended to other materials. Figure 29c shows the CdSe nanoparticle bound to pIII, but not at pVIII. Because more than one streptavidin (tetrameric (4×13 kDa) protein) can be conjugated to nanoparticles, complex structure could be expected by bridging phage particles. Linearly and Y-shaped structures are shown in Figure 29d and e as examples.

5.5. Conclusion

A type 8 phage library was successfully applied for selection against Au surface to assemble Au nanoparticles on the selected phage. The assembly results in densely aligned Au nanoparticles, forming wire-like structures. In addition, Type 83 phage which display both Au binding peptide at pVIII and streptavidin binding peptide at pVIII were constructed and applied for programmable assembly of Au nanoparticles and streptavidin conjugated particles (Au and CdSe). This rational approach could be easily extended to bottom-up assembly of other nanoscale materials. In addition to pIII and pVIII, pIX proteins can be modified to display peptides. Therefore further genetic engineering of phage could challenge assembly with more complex geometries using phage as a nanoscale template and building block.

CHAPTER 6: Summary and Conclusions

Surface display of peptides on phage enables the assembly of foreign molecules on their cylindrical body (pVIII) and tip (pIII) due to interaction between the peptides and the target molecules. Genetically engineered type 8 and type 83 phage were constructed and used for application in biotechnology and inorganic nanotechnology in this thesis, chapters 2 through 5: (chapter 2) cobalt ion mediated self-assembly of genetically engineered bacteriophage for biomimetic Co-Pt hybrid material, (chapter 3) phage displayed peptide selection for TiO₂ in a non-biological environment. (chapter 4) Alignment and storage of biological molecules in phage films, and (chapter 5) Assembly of inorganic nanoparticles using genetically engineered bacteriophage.

In chapter 2, genetically modified type 8 phage particles having affinity to cobalt ions were selected and used for the metal-ion mediated bundle at low phage concentrations. The phage bundles with a sponge-like morphology were used as a template to nucleate Co-Pt nanoparticles. The nanoparticles were regularly located on the phage structure with a narrow size distribution. The hybrid bio-inorganic material showed superparamagnetic properties with high anisotropy.

In chapter 3, Ethanol resistant phage were selected using a type 8 phage library. Then, a pIII peptide library was constructed by genetic engineering of the ethanol resistant phage to select a binder to TiO₂ in ethanol environment (90% ethanol). The selected peptide was used for growth control of TiO₂ during general sol-gel synthesis, resulting in the formation of individual spherical particles (~ 60 nm) without gelation process.

In chapter 4, β -galactosidase and GFPuv were successfully stored in smectically ordered phage films. Carbohydrates (glucose/sucrose) were used as a stabilizer to increase stability of the protein in the film. Type 3 phage, which displays S1 peptide (streptavidin binding peptide), was employed for alignment of streptavidin conjugated phycoerythrin in phage films. The alignment could be helpful to distribute the phycoerythrin regularly through the film. Also, it is possible that the alignment reduces degradation of proteins during the drying process.

Finally in chapter 5, Au nanoparticles were assembled on type 8 phage which display Au binding peptide at pVIII. Densely aligned Au nanoparticles on a phage particle formed wire-like structures. In addition, Type 83 phage which display both Au binding peptide at pVIII and streptavidin binding peptide at pVIII were applied for assembly of both Au nanoparticles and streptavidin conjugated particles (Au and CdSe) at different positions on the phage particles.

Genetic engineering of bacteriophage by displaying peptides or proteins (at pIII, pVIII, and pIX) could have tremendous application in biotechnology, nanotechnology, and material science. Because the length of filamentous bacteriophage can be adjusted in

addition to peptide display, bacteriophage could provide a tunable nanoscale biological building block. For further development in biomimetic inorganic nanomaterials, the mechanism of interactions between biological molecules (DNA, peptide, and proteins) and inorganic surfaces should be elucidated. Nucleation of inorganics on biological matrix was known to be controlled by supersaturation level of inorganic precursors and reduction of interfacial energy between the matrix and water.[63] High binding affinity of biological matrix to inorganic precursors could increase local concentration of the precursors near the matrix. Binding affinity to the precursors could affect on interfacial energy. Effects of binding affinities on local concentration near the matrix and the interfacial energy for biomineralization could be interesting studies near future. Biocompatible and biologically degradable functional materials using genetically engineered phage could be one of the potential applications. I believe that the genetically engineered phage will be studied and applied more for innovative materials with excellent properties due to their multiple peptide display systems.

Appendix A: construction for M13SK

M13SK phage vector (Figure A1) was constructed for genetic engineering of both pIII and pVIII by modifying M13KE phage vector (NEB) as described previously.[13] T at position 1372 and C at position 1381 was mutated to A and G respectively by using overlap extension PCR.

Region from position 1179 to 1395 was amplified with primers 5'-M13KE-1179 (5'-GCTTGGTATAATCGCTGG-3') and 3'-M13KEmu-p8 (5'-GCTTTTGCGGGATC CTCACCC TCTGCAGCGAAAGACAG-3'). Region from position 1358 to 2277 was also amplified with primers 5'-M13KEmu-p8 (5'-CTG TCT TTC GCT GCA GAG GGT GAG GAT CCC GCA AAA GC-3') and 3'-M13KE-2 (5'-GAC AGG AGG TTG AGG CAG-3'). The amplified product of region from position 1179 to 2277 were obtained by performing additional PCR reaction with mixture of the two PCR products, 5'-M13KE-1179, and 3'-M13KE-2 (Figure A2). The final PCR product and M13KE vector was digested by BspH I and Acc65 I, and ligated into M13KE vector. After transfection using XL1-Blue supercompetent cells (Stratagen), 100 µl of the cells were plated with 3ml of agaros top. Plaques were selected and sequenced to confirm the mutation. the *Pst* I site at position 6246 was deleted by mutating T to A at position 6250 by using same method. One PCR product were obtained with primer 5'-M13KE-5785 (5'-GTG GAC TCT TGT TCC AAA CTG-3') and 3'-M13KEmu-6250 (5'-CAG TGA ATT CGA GGA CCA GCA GGC ATG CAA GCT TG-3'), and the other PCR product were obtained with primer 5'-M13KEmu-6250 (5'-CAA GCT TGC ATG CCT GCT GGT CCT CGA ATT CAC TG-3') and 3'-M13KE-7175 (5'-

CAA TAA AGC CTC AGA GCA TAA AGC-3'). The two region was extended and amplified with primer 5'-M13KE-5785 and 3'-M13KE-7175. The PCR product was digested with Hind III and Bgl II, and ligated into digested dsDNA of the mutant M13KE vector which contain mutation at pVIII sites.

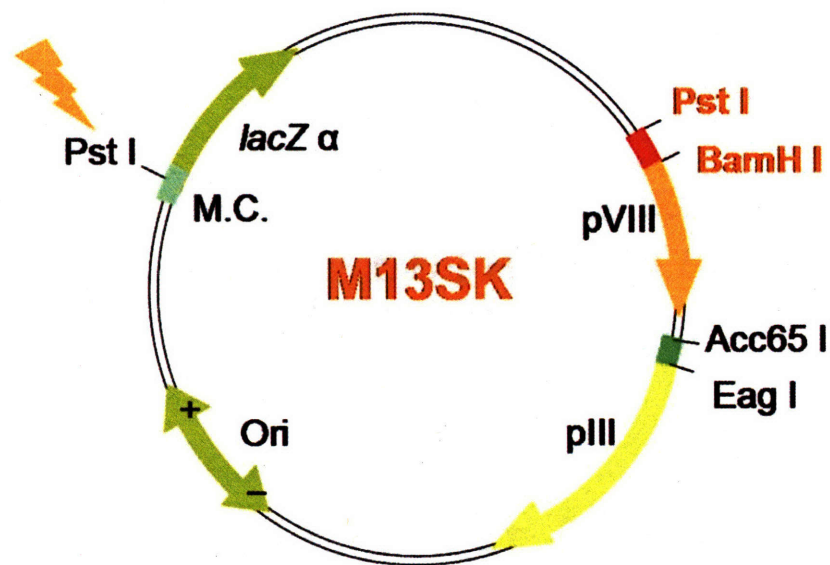


Figure A1. Restriction site map of M13SK. M13KE vector was modified. *Pst I* and *BamHI I* sites were added, and *Pst I* at Multi cloning site was deleted.

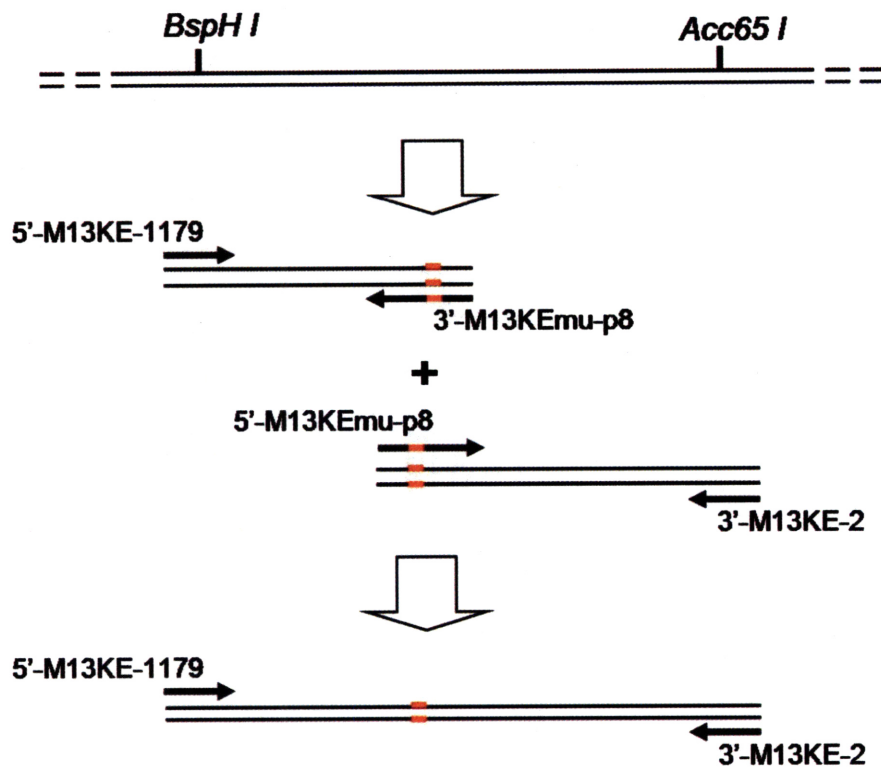


Figure A2. Overlap extension PCR for pVIII cloning sites. Two individual PCR products with mutation sites were obtained. The two PCR products were extended and amplified with 5'-M13KE-1179 and 3'-M13KE-2 primers.

Appendix B: construction of type 83 phage

The region from position 1358 to 2277 of the type 3 dsDNA, which contains selected peptide sequence at pIII, was amplified using PCR with primer 5'-M13KEmu-p8 (5'-CTGTCTTTCGCTGCAGAGGGTGAGGGATCCCGCAAAGC-3') and 3'-M13KE-2 (5'-CACCGTTCATCTGTCCTC-3'). *Pst* I and *Bam*H I restriction sites for pVIII cloning can be generated, because 5'-M13KEmu-p8 primer contains mutation sites for the restriction sites. Table B1 show the details of the PCR reaction.

Table B1. PCR of type 3 phage for construction of type 83 phage

ddH ₂ O	75 μ l
10X Pfu PCR buffer	10 μ l
2.5 mM dNTPs	8 μ l
5'-M13KEmu-p8 (10 μ M)	2 μ l
3'-M13KE-2 (10 μ M)	2 μ l
Pfu polymerase (2.5 U/ μ)	2 μ l
dsDNAor ssDNA of type 3 phage (10 nm/ μ l)	1 μ l

* Annealing temperature = 50 °C, extension time = 1 min

The PCR products (insert) and dsDNA of type 8 phage (vector) were digested with *Bam*H I and *Eag* I. After gel-purification by running electrophoresis using 1% agarose gel,

The insert and vector were ligated by incubation with T4 DNA ligase (NEB) at 16 °C for overnight. The mixture of ligation was transfected into XL1-Blue supercompetent cells (Stratagen) (Figure B1). After 30 min incubation at 37 °C, 100 µl of the transfected cells were plated with 3 ml of agarose-top. Each plaque was inoculated and amplified to confirm its DNA sequence.

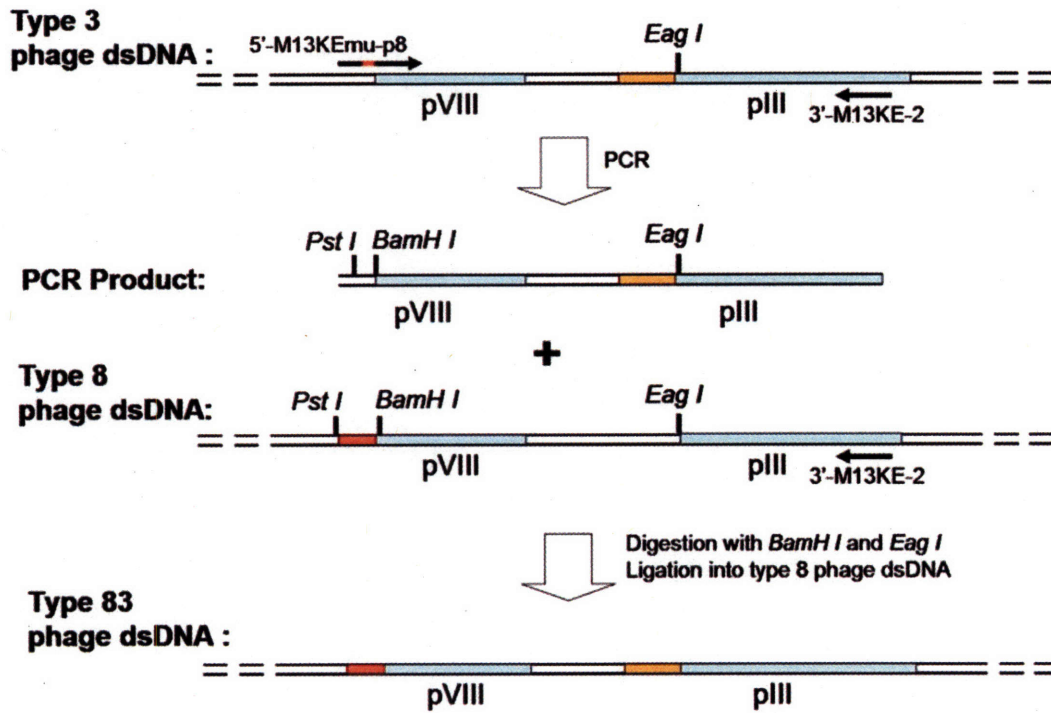


Figure B1. Construction of Type 83 phage. PCR product which contains *Pst I* and *BamH I* restriction site was obtained. The region between *BamH I* and *Eag I* was cloned to type 8 phage dsDNA. The dsDNA of type 83 phage contains DNA sequence for peptide display at both pIII (orange) and pVIII (red).

References and Notes

1. Yan, H., et al., *DNA-templated self-assembly of protein arrays and highly conductive nanowires*. Science, 2003. **301**(5641): p. 1882-1884.
2. Vauthey, S., et al., *Molecular self-assembly of surfactant-like peptides to form nanotubes and nanovesicles*. Proceedings of the National Academy of Sciences of the United States of America, 2002. **99**(8): p. 5355-5360.
3. Petka, W.A., et al., *Reversible hydrogels from self-assembling artificial proteins*. Science, 1998. **281**(5375): p. 389-392.
4. Wayne Shenton, T.D., Mark Young, Gerald Stubbs, and Stephen Mann, *Inorganic-Organic Nanotube Composites from Template Mineralization of Tobacco Mosaic Virus*. Advanced Materials, 1999. **11**(3): p. 253-256.
5. Young, T.D.a.M., *Virus Particles as Templates for Materials Synthesis*. Advanced Materials, 1999. **11**(8): p. 679-681.
6. Whaley, S.R., et al., *Selection of peptides with semiconductor binding specificity for directed nanocrystal assembly*. Nature, 2000. **405**(6787): p. 665-668.
7. Naik, R.R., et al., *Biomimetic synthesis and patterning of silver nanoparticles*. Nature Materials, 2002. **1**(3): p. 169-172.
8. Lee, S.W., et al., *Ordering of quantum dots using genetically engineered viruses*. Science, 2002. **296**(5569): p. 892-895.

9. Specthrie, L., et al., *Construction of a microphage variant of filamentous bacteriophage*. J Mol Biol, 1992. **228**(3): p. 720-4.
10. Mao, C., et al., *Viral assembly of oriented quantum dot nanowires*. Proc Natl Acad Sci U S A, 2003. **100**(12): p. 6946-51.
11. Mao, C., et al., *Virus-based toolkit for the directed synthesis of magnetic and semiconducting nanowires*. Science, 2004. **303**(5655): p. 213-7.
12. Flynn, C.E., et al., *Synthesis and organization of nanoscale II-VI semiconductor materials using evolved peptide specificity and viral capsid assembly*. Journal of Materials Chemistry, 2003. **13**(10): p. 2414-2421.
13. Petrenko, V.A., et al., *A library of organic landscapes on filamentous phage*. Protein Engineering, 1996. **9**(9): p. 797-801.
14. Yu, S.M., et al., *Smectic ordering in solutions and films of a rod-like polymer owing to monodispersity of chain length*. Nature, 1997. **389**(6647): p. 167-70.
15. Lee, S.W., B.M. Wood, and A.M. Belcher, *Chiral smectic C structures of virus-based films*. Langmuir, 2003. **19**(5): p. 1592-1598.
16. Dogic, Z. and S. Fraden, *Smectic phase in a colloidal suspension of semiflexible virus particles*. Physical Review Letters, 1997. **78**(12): p. 2417-2420.
17. Deegan, R.D., et al., *Capillary flow as the cause of ring stains from dried liquid drops*. Nature, 1997. **389**(6653): p. 827-829.
18. Huang, Y., et al., *Directed assembly of one-dimensional nanostructures into functional networks*. Science, 2001. **291**(5504): p. 630-3.

19. Lee, S.W., S.K. Lee, and A.M. Belcher, *Virus-based alignment of inorganic, organic, and biological nanosized materials*. *Advanced Materials*, 2003. **15**(9): p. 689-692.
20. Zhou, M., D. Bentley, and I. Ghosh, *Helical supramolecules and fibers utilizing leucine zipper-displaying dendrimers*. *J Am Chem Soc*, 2004. **126**(3): p. 734-5.
21. Wang, C., R.J. Stewart, and J. Kopecek, *Hybrid hydrogels assembled from synthetic polymers and coiled-coil protein domains*. *Nature*, 1999. **397**(6718): p. 417-20.
22. Petka, W.A., et al., *Reversible hydrogels from self-assembling artificial proteins*. *Science*, 1998. **281**(5375): p. 389-92.
23. Schneider, J.P., et al., *Responsive hydrogels from the intramolecular folding and self-assembly of a designed peptide*. *J Am Chem Soc*, 2002. **124**(50): p. 15030-7.
24. Qiu, Y. and K. Park, *Environment-sensitive hydrogels for drug delivery*. *Adv Drug Deliv Rev*, 2001. **53**(3): p. 321-39.
25. Miyata, T., N. Asami, and T. Uragami, *A reversibly antigen-responsive hydrogel*. *Nature*, 1999. **399**(6738): p. 766-9.
26. Klabunde, K.J., *Nanoscale Materials in Chemistry*. 2001, New York: John Wiley & Sons, Inc.

27. Chemseddine, A. and T. Moritz, *Nanostructuring titania: Control over nanocrystal structure, size, shape, and organization*. European Journal of Inorganic Chemistry, 1999(2): p. 235-245.
28. Cozzoli, P.D., A. Kornowski, and H. Weller, *Low-temperature synthesis of soluble and processable organic-capped anatase TiO₂ nanorods*. Journal of the American Chemical Society, 2003. **125**(47): p. 14539-14548.
29. Jiang, X.C., T. Herricks, and Y.N. Xia, *Monodispersed spherical colloids of titania: Synthesis, characterization, and crystallization*. Advanced Materials, 2003. **15**(14): p. 1205-+.
30. Boury, B. and R.J. Corriu, *Auto-organisation of hybrid organic-inorganic materials prepared by sol-gel process*. Chem Commun (Camb), 2002(8): p. 795-802.
31. Klabunde, K.J., *Nanoscale materials in chemistry*. 2001.
32. Zarur, A.J. and J.Y. Ying, *Reverse microemulsion synthesis of nanostructured complex oxides for catalytic combustion*. Nature, 2000. **403**(6765): p. 65-7.
33. Kroger, N., R. Deutzmann, and M. Sumper, *Polycationic peptides from diatom biosilica that direct silica nanosphere formation*. Science, 1999. **286**(5442): p. 1129-32.
34. Luckarift, H.R., et al., *Enzyme immobilization in a biomimetic silica support*. Nat Biotechnol, 2004. **22**(2): p. 211-3.

35. Cha, J.N., et al., *Biomimetic synthesis of ordered silica structures mediated by block copolypeptides*. Nature, 2000. **403**(6767): p. 289-92.
36. Amako, K. and K. Yasunaka, *Ether induced morphological alteration of Pf-1 filamentous phage*. Nature, 1977. **267**(5614): p. 862-3.
37. Holliger, P., L. Riechmann, and R.L. Williams, *Crystal structure of the two N-terminal domains of g3p from filamentous phage fd at 1.9 angstrom: Evidence for conformational lability*. Journal of Molecular Biology, 1999. **288**(4): p. 649-657.
38. Petrenko, V.A., et al., *A library of organic landscapes on filamentous phage*. Protein Eng, 1996. **9**(9): p. 797-801.
39. Olofsson, L., et al., *Filamentous bacteriophage stability in non-aqueous media*. Chem Biol, 2001. **8**(7): p. 661-71.
40. Buhro, W.E. and V.L. Colvin, *Semiconductor nanocrystals: Shape matters*. Nat Mater, 2003. **2**(3): p. 138-9.
41. Liang-Shi Li, J.H., Weidong Yang, and A. Paul Alivisatos, *Band Gap Variation of Size- and Shape-Controlled Colloidal CdSe Quantum Rods*. Nano Letters, 2001. **1**(7): p. 349-351.
42. Leslie-Pelecky, D.L., *Magnetic Properties of Nanostructured Materials*. Chemistry of Materials, 1996. **8**: p. 1770-1783.
43. Weiner, S., W. Traub, and H.D. Wagner, *Lamellar bone: Structure-function relations*. Journal of Structural Biology, 1999. **126**(3): p. 241-255.

44. Weiner, S. and H.D. Wagner, *The material bone: Structure mechanical function relations*. Annual Review of Materials Science, 1998. **28**: p. 271-298.
45. Cha, J.N., et al., *Silicatein filaments and subunits from a marine sponge direct the polymerization of silica and silicones in vitro*. Proceedings of the National Academy of Sciences of the United States of America, 1999. **96**(2): p. 361-365.
46. Shimizu, K., et al., *Silicatein alpha: Cathepsin L-like protein in sponge biosilica*. Proceedings of the National Academy of Sciences of the United States of America, 1998. **95**(11): p. 6234-6238.
47. Hirano, S., et al., *The preparation and applications of functional fibres from crab shell chitin*. Journal of Biotechnology, 1999. **70**(1-3): p. 373-377.
48. Falini, G., et al., *Control of aragonite or calcite polymorphism by mollusk shell macromolecules*. Science, 1996. **271**(5245): p. 67-69.
49. Shen, X.Y., et al., *Molecular cloning and characterization of hustrin A, a matrix protein from shell and pearl nacre of Haliotis rufescens*. Journal of Biological Chemistry, 1997. **272**(51): p. 32472-32481.
50. Lin, X.M., et al., *Control of cobalt nanoparticle size by the germ-growth method in inverse micelle system: Size-dependent magnetic properties*. Journal of Materials Research, 1999. **14**(4): p. 1542-1547.
51. Kim, D.K., et al., *Synthesis and characterization of surfactant-coated superparamagnetic monodispersed iron oxide nanoparticles*. Journal of Magnetism and Magnetic Materials, 2001. **225**(1-2): p. 30-36.

52. Kumar, D., et al., *Synthesis and atomic-level characterization of Ni nanoparticles in Al₂O₃ matrix*. Applied Physics Letters, 2002. **81**(22): p. 4204-4206.
53. Xing, G. and V.J. DeRose, *Designing metal-peptide models for protein structure and function*. Current Opinion in Chemical Biology, 2001. **5**(2): p. 196-200.
54. Lombardi, A., et al., *Retrostructural analysis of metalloproteins: Application to the design of a minimal model for diiron proteins*. Proceedings of the National Academy of Sciences of the United States of America, 2000. **97**(12): p. 6298-6305.
55. Muthukumar, M., C.K. Ober, and E.L. Thomas, *Competing interactions and levels of ordering in self-organizing polymeric materials*. Science, 1997. **277**(5330): p. 1225-1232.
56. Huang, Y.H., et al., *Hysteresis behavior of CoPt nanoparticles*. Ieee Transactions on Magnetics, 2002. **38**(5): p. 2604-2606.
57. Petit, C., S. Rusponi, and H. Brune, *Magnetic properties of cobalt and cobalt-platinum nanocrystals investigated by magneto-optical Kerr effect*. Journal of Applied Physics, 2004. **95**(8): p. 4251-4260.
58. Mao, C.B., et al., *Viral assembly of oriented quantum dot nanowires*. Proceedings of the National Academy of Sciences of the United States of America, 2003. **100**(12): p. 6946-6951.

59. Reiss, B.D., et al., *Biological routes to metal alloy ferromagnetic nanostructures*. Nano Letters, 2004. **4**(6): p. 1127-1132.
60. Shapiro, A.L., et al., *Growth-induced magnetic anisotropy and clustering in vapor-deposited Co-Pt alloy films*. Physical Review B, 1999. **60**(18): p. 12826-12836.
61. Hickey, B.J., et al., *Enhanced magnetic anisotropy energy density for superparamagnetic particles of cobalt*. Physical Review B, 1996. **53**(1): p. 32-33.
62. Mejia-Lopez, J., P. Soto, and D. Altbir, *Asymmetric reversal of the hysteresis loop in exchange-biased nanodots*. Physical Review B, 2005. **71**(10): p. 104422.
63. Mann, S., *Bioinorganic Chemistry: Principles and Concepts in Bioinorganic Materials Chemistry*. 2001, New York: Oxford University Press. 38-67.
64. Brown, S., *Metal-recognition by repeating polypeptides*. Nature Biotechnology, 1997. **15**(3): p. 269-272.
65. Sarikaya, M., et al., *Molecular biomimetics: nanotechnology through biology*. Nature Materials, 2003. **2**(9): p. 577-585.
66. Li, M., *Applications of display technology in protein analysis*. Nature Biotechnology, 2000. **18**(12): p. 1251-1256.
67. Boury, B. and R.J.P. Corriu, *Auto-organisation of hybrid organic-inorganic materials prepared by sol-gel process*. Chemical Communications, 2002(8): p. 795-802.

68. Sumerel, J.L., et al., *Biocatalytically templated synthesis of titanium dioxide*. *Chemistry of Materials*, 2003. **15**(25): p. 4804-4809.
69. Bansal, V., et al., *Fungus-mediated biosynthesis of silica and titania particles*. *Journal of Materials Chemistry*, 2005. **15**(26): p. 2583-2589.
70. Linsebigler, A.L., G.Q. Lu, and J.T. Yates, *Photocatalysis on Tio₂ Surfaces - Principles, Mechanisms, and Selected Results*. *Chemical Reviews*, 1995. **95**(3): p. 735-758.
71. Lee, S.K., D.S. Yun, and A.M. Belcher, *Cobalt ion mediated self-assembly of genetically engineered bacteriophage for biomimetic Co-Pt hybrid material*. *Biomacromolecules*, 2006. **7**(1): p. 14-17.
72. Scofield, J.H., *Hartree-Slater Subshell Photoionization Cross-Sections at 1254 and 1487ev*. *Journal of Electron Spectroscopy and Related Phenomena*, 1976. **8**(2): p. 129-137.
73. Willett, R.L., et al., *Differential adhesion of amino acids to inorganic surfaces*. *Proceedings of the National Academy of Sciences of the United States of America*, 2005. **102**(22): p. 7817-7822.
74. Akerlof, G., *Dielectric constants of some organic solvent-water mixtures at various temperatures*. *The Journal of the American Chemical Society*, 1932. **54**(11): p. 4125-4139.
75. Hench, L.L. and J.K. West, *The Sol-Gel Process*. *Chemical Reviews*, 1990. **90**(1): p. 33-72.

76. Erdem, B., et al., *XPS and FTIR surface characterization of TiO₂ particles used in polymer encapsulation*. *Langmuir*, 2001. **17**(9): p. 2664-2669.
77. Simmons, G.W. and B.C. Beard, *Characterization of Acid-Base Properties of the Hydrated Oxides on Iron and Titanium Metal-Surfaces*. *Journal of Physical Chemistry*, 1987. **91**(5): p. 1143-1148.
78. Hansson, K.M., et al., *Whole blood coagulation on protein adsorption-resistant PEG and peptide functionalised PEG-coated titanium surfaces*. *Biomaterials*, 2005. **26**(8): p. 861-872.
79. Sun, W.Q. and P. Davidson, *Protein inactivation in amorphous sucrose and trehalose matrices: effects of phase separation and crystallization*. *Biochimica Et Biophysica Acta-General Subjects*, 1998. **1425**(1): p. 235-244.
80. Davidson, P. and W.Q. Sun, *Effect of sucrose/raffinose mass ratios on the stability of co-lyophilized protein during storage above the T-g*. *Pharmaceutical Research*, 2001. **18**(4): p. 474-479.
81. Perez, C., et al., *Recent trends in stabilizing protein structure upon encapsulation and release from bioerodible polymers*. *Journal of Pharmacy and Pharmacology*, 2002. **54**(3): p. 301-313.
82. Seung-Wuk Lee, B.M.W., and Angela M. Belcher, *Chiral Smectic C Structures of Virus-Based Films*. *Langmuir*, 2003. **19**: p. 1592-1598.

83. Sousa, R., *Use of Glycerol, Polyols and Other Protein-Structure Stabilizing Agents in Protein Crystallization*. Acta Crystallographica Section D-Biological Crystallography, 1995. **51**: p. 271-277.
84. Flynn, C.E., et al., *Viruses as vehicles for growth, organization and assembly of materials*. Acta Materialia, 2003. **51**(19): p. 5867-5880.
85. Sarikaya, M., et al., *Molecular biomimetics: nanotechnology through biology*. Nat Mater, 2003. **2**(9): p. 577-85.